Spring 2020

Comparing the bioavailability of a natural and synthetic iron source: Do past experiments accurately model phytoplankton response to episodic iron addition?

Clayton Mazur
c.mazur24@comcast.net

Comparing the bioavailability of a natural and synthetic iron source: Do past experiments accurately model phytoplankton response to episodic iron addition?

By

Clayton Moore Mazur

Accepted in Partial Completion
of the Requirements for the Degree
Master of Science

ADVISORY COMMITTEE

Dr. Suzanne Strom, Chair

Dr. Brian Bingham

Dr. Brady Olson

GRADUATE SCHOOL

David L. Patrick, Dean

Master's Thesis

In presenting this thesis in partial fulfillment of the requirements for a master's degree at Western Washington University, I grant to Western Washington University the non-exclusive royalty-free right to archive, reproduce, distribute, and display the thesis in any and all forms, including electronic format, via any digital library mechanisms maintained by WWU.

I represent and warrant this is my original work and does not infringe or violate any rights of others. I warrant that I have obtained written permissions from the owner of any third party copyrighted material included in these files.

I acknowledge that I retain ownership rights to the copyright of this work, including but not limited to the right to use all or part of this work in future works, such as articles or books.

Library users are granted permission for individual, research and non-commercial reproduction of this work for educational purposes only. Any further digital posting of this document requires specific permission from the author.

Any copying or publication of this thesis for commercial purposes, or for financial gain, is not allowed without my written permission.

Clayton Mazur

19 June 2020

Comparing the bioavailability of a natural and synthetic iron source: Do past experiments accurately model phytoplankton response to episodic iron addition?

A Thesis
Presented to
The Faculty of
Western Washington University

In Partial Fulfillment
Of the Requirements for the Degree
Master of Science

by
Clayton Moore Mazur
June, 2020

ABSTRACT

Episodic iron input from natural sources (e.g., riverine input, dust deposition, and mesoscale eddies) plays an important role in dictating phytoplankton growth, physiology, and community structure in the high-nitrate low-chlorophyll (HNLC) waters of the Northern Gulf of Alaska (NGA). Iron addition experiments utilizing the synthetic iron source, $FeCl_3$, have been performed in all major HNLC regions and have resulted in diatom blooms with significant implications for ecosystem productivity and resilience. If $FeCl_3$ and natural iron sources differ in bioavailability, and hence potential phytoplankton production, re-interpretation of these results is warranted. To test the hypothesis that natural and synthetic iron sources are differentially bioavailable, we performed a deck-board iron addition experiment in the summer of 2019. We exposed the NGA HNLC phytoplankton community to three iron sources: $FeCl_3$, the Copper River plume, and an HNLC control and assessed net growth, photosynthetic efficiency, community composition, and nutrient use over a 5 d incubation. Addition of the $FeCl_3$ and Copper River plume iron sources alleviated iron stress for the total phytoplankton community, yet the bioavailability of these two iron sources was size-dependent. Cells > 20 µm responded differently to all three iron sources, with net growth rates and photosynthetic efficiency being highest in the $FeCl_3$ treatment and intermediate in the Copper River plume treatment. In contrast to cells > 20 µm, phytoplankton < 20 µm responded similarly to the Copper River plume and $FeCl_3$ treatments. Consistent with previous experiments, $FeCl_3$ addition promoted diatom growth. However, the Copper River plume iron source primarily increased the production and turnover of cells < 20 µm. We conclude that diatom growth and physiology measured in previous iron addition experiments in response to $FeCl_3$ do not directly translate to fluvial iron sources. We also suggest that fluvial iron input is critical to maintaining ultraplankton in NGA

HNLC waters and that it may aid the rapid transport of biomass into secondary production with the addition of more highly bioavailable iron sources.

AWKNOWLEDGEMENTS

I would like to extend a deep appreciation to my thesis advisor, Dr. Suzanne Strom, for her mentorship, support, and positive spirit. I would also like to thank our collaborator, Dr. Ana Aguilar-Islas, for her trace metal chemistry expertise and collaborate spirit. It was a joy to work with these experts and without their encouragement and shared knowledge, this thesis would not be possible. I also want to thank my committee members, Dr. Brian Bingham and Dr. Brady Olson, for their guidance through statistics and critical feedback that greatly improved this thesis. Special thanks to Kelley Bright and Kerri Fredrickson, for their dedicated time and energy to train me in flow cytometry and microscopy techniques. I also want to thank Celia Ross, whose micrograzer counts enhanced the story I am able to tell in this thesis. I would like to extend a sincere thanks to Hana Busse, Annie Kandel, Carrie Brown, and Kelsie Maslen for help with experimental setup and for their camaraderie while at sea. I would like to thank Jay Diamond, Amy Fotheringham, Aletha Macomber, and Gene McKeen for logistical support during methods developments and travel to AK. I would also like to thank the captain and crew of the *R/V Sikuliaq*. Finally, I would like to acknowledge my family for their morale, support, and patience through this endeavor. This work was funded by NSF (grants 1656070 and 1434842), NPRB (grant NA15MF4720173), and Western Washington University.

TABLE OF CONTENTS

LIST OF TABLES

LIST OF FIGURES

INTRODUCTION

The Northern Gulf of Alaska (NGA) as a Hotspot for Biological Productivity

The NGA is a rich ecoregion of the world's oceans in which seasonal cycles in resource availability drive blooms of microscopic algae called phytoplankton (Lagerloef 1995; Stabeno et al. 2004). Superimposed on this seasonality is high interannual variability associated with global forcing events (e.g., El Niño). NGA phytoplankton productivity forms the base of the marine food web, affects distributions of critical prey species (e.g., copepods and capelin; Liu et al. 2005; Shultz et al. 2009), and supports economically important fisheries (Anderson and Piatt 1999; Sumaila et al. 2011). Therefore, factors affecting phytoplankton growth and physiology are critical to understanding the high productivity of the NGA ecosystem.

Seasonal cycles in resource availability contribute to large-scale spatiotemporal variability in phytoplankton biomass and community composition in the NGA (Brickley and Thomas 2004; Strom et al. 2006; Waite and Mueter 2013). In the spring, when downwelling-favorable winds are strong and promote vertical mixing, phytoplankton blooms are dominated by large-celled diatoms (e.g. *Thalassiosira* and *Chaetoceros*; Strom et al. 2016). In summer, with the onset of stratification and nutrient depletion at depths < 20 m, communities become dominated by *Synechococcus* sp., a photosynthetic bacteria, as well as flagellates < 10 μm in size (Strom, unpublished data). Fall communities are often dominated by these small algae and diatom abundance becomes highly variable. During all seasons, phytoplankton distributions across the shelf follow gradients in dissolved nutrients, particularly iron (Strom et al. 2006; Wu et al. 2009). Despite general seasonality in phytoplankton biomass, interannual temporal-spatial variability exists with respect to bloom

timing, intensity, duration, and resource utilization (Henson 2007; Waite and Mueter 2013). Because of environmental heterogeneity, phytoplankton blooms are controlled by a variety of bottom-up (growth rate limiting) and top-down (biomass eliminating) regulatory processes that remain incompletely characterized.

Iron availability is one of the most important mechanisms controlling primary production in the NGA (e.g. Martin et al. 1989; Boyd et al. 2004). Off the continental shelf, the oceanic waters of the NGA have been classified as high-nitrate low-chlorophyll (HNLC), and phytoplankton blooms are less common in this region due to iron limitation (Martin and Fitzwater 1988; Hutchins and Bruland 1998; Boyd et al. 2004). However, the nature of this limitation is complex due to episodic iron input across the region. Atmospheric dust and anthropogenic aerosol deposition may be the primary allochthonous source of the oceanic North Pacific's iron (Moore et al. 1984; Duce 1986; Duce and Tindale 1991a; Aguilar-Islas et al. 2010). A single dust event in 2006 deposited 25 – 80 ktons of Fe into the NGA, of which 30 – 200 tons was soluble (Crusius et al. 2011). During atmospheric transport, aerosolized Fe(III) complexes may be reduced to labile forms by photochemical processes (Donaghay et al. 1991; Duce and Tindale 1991b), contributing to the bioavailability of terrigenous iron to phytoplankton (Young et al. 1991; Mackey et al. 2012; Achterberg et al. 2013). Freshwater input from large point sources (e.g. the Copper River; Aguilar-Islas et al. 2016) and glacial discharge (Lippiatt et al. 2010) peaks between June and September and carries with it large suspended sediment loads ($> 70 \times 10^6$ tons yr^{-1}; Milliman and Syvitski 1992). Iron constitutes ~ 4 % of the sediment load, by weight, making freshwater input a major source of allochthonous iron to the NGA (Wu et al. 2009). Despite large concentrations of iron flowing into the NGA, the Alaska Coastal Current constrains much of the fluvial iron input to coastal waters (Wu et al. 2009) and establishes cross-

shelf gradients in dissolved iron concentrations. Cross-shelf gradients in phytoplankton distribution in the NGA are expected to be correlated with the distribution of dissolved iron (Strom et al. 2006), but the bioavailability of fluvial iron inputs and their role in dictating phytoplankton community composition remain incompletely characterized. In summer when the downwelling winds relax, inflow of deep offshore waters charges coastal waters with nutrients, including iron. Upwelling events infrequently occur during summer, but when they do, they may sporadically deliver subsurface iron to the euphotic zone (Stabeno et al. 2004; Whitney et al. 2005; Ladd et al. 2005). Finally, mesoscale eddy propagation across the NGA shelf break may enhance phytoplankton growth in HNLC waters. Eddies originating near Sitka and Yakutat promote upwelling on their leading and trailing edges, entrain and transport iron-rich coastal water to the HNLC region, and promote cross-shelf exchange (Okkonen et al. 2003; Lippiatt et al. 2010). Iron sourced to the HNLC waters from eddies can persist for several years and contribute sporadically to phytoplankton productivity (Whitney et al. 2005).

Iron availability acts as an important bottom-up regulator of phytoplankton productivity. The relative bioavailability of the terrigenous, subsurface (i.e. deep shelf), and synthetic iron sources has not been established. Different iron sources may differentially influence phytoplankton growth rates and primary production in the NGA. In this way, both the amount and source of iron act as bottom up regulators of phytoplankton and dictate NGA phytoplankton community composition and the magnitude of phytoplankton blooms.

Bottom-up Bloom Regulation: Proximal Physiological Effects of Iron Limitation

The reduction-oxidation reactivity of inorganic iron makes it a versatile and necessary component of many metabolic pathways (Morel et al. 1991). Iron is vital for cofactors, cellular respiration, photosynthesis and associated light- harvesting pigments, and reactive oxygen species (ROS) regulation (Morel et al. 1991; Geider and La Roche 1994). Given the importance of iron in mediating metabolism in plants, iron limitation in the NGA phytoplankton community is expected to have significant effects on primary production.

Phytoplankton show great plasticity in biochemical composition, nutrient utilization, and photosynthetic efficiencies (Morel et al. 1991), yet iron limitation elicits sustained physiological harm to phytoplankton cells. Chlorosis, a decrease in cellular chlorophyll *a* content, has been documented for both *Synechococcus* sp. and eukaryotic phytoplankton exposed to limiting iron (Rueter and Ades 1987; Doucette and Harrison 1990; Greene et al. 1991, 1992). Essential pigment-binding proteins, cytochromes, and D1 proteins (a key protein in the photosystem II reaction center) also decrease in these phytoplankton (Glover 1977; Guikema and Sherman 1983). Damage to the photosynthetic apparatus, diagnosed by declines in photosynthetic efficiency, occurs in iron limited phytoplankton both in culture and *in situ*. Photosynthetic efficiency is a measure of how well photosystem II transfers electrons in the photosynthetic pathway and reflects the ability of phytoplankton cells to harvest light for carbon fixation (Krause and Weis 1984). Declines in photosynthetic efficiency have been documented for many iron-starved phytoplankton in culture including *Synechococcu*s sp. (Guikema and Sherman 1983), chlorophytes (Rueter and Ades 1987; Greene et al. 1992), and diatoms (Greene et al. 1991, 1992; Allen et al. 2008; Sunda and Huntsman 2011). Iron addition to phytoplankton communities in the Southern Ocean (Olson et al. 2000; Boyd et al. 2004) and equatorial Pacific

(Behrenfeld et al. 1996) resulted in increases in photosynthetic efficiency over the course of several days, indicating widespread iron limitation in these HNLC regions. After iron was added to starved cultures of *Dunaliella tertiolecta*, photosynthetic recovery occurred in three stages over a period of > 18 h (Greene et al. 1992), indicating that iron starvation may have significant effects on HNLC phytoplankton production.

ROS also acts as a bottom-up regulator of phytoplankton growth during iron limitation. The production of ROS (e.g., superoxide ($^{\bullet}O_2^-$), hydrogen peroxide (H_2O_2), and hydroxyl radical ($^{\bullet}OH$)) occurs during cellular respiration, photo-oxidation of photosystem II reaction centers, or via the Mehler reaction (Salin 1988). ROS are vital components of intracellular signaling cascades, gene regulation pathways, and antiviral defenses (Apel and Hirt 2004; Liu et al. 2007). However, left unchecked, ROS can degrade lipid bilayers, alter protein structures, and mutate DNA (Lesser 2006). Phytoplankton naturally regulate ROS by synthesizing scavenging antioxidants such as Fe-superoxide dismutase, catalase, and peroxidase (Canini et al. 1992; Geider and La Roche 1994; Martínez 2007) and by synthesizing non-enzymatic anti-oxidants (e.g. ascorbate, various pigments; Mallick and Mohn 2000). Under iron-limiting conditions, production of iron-containing antioxidants is impaired and the ability of cells to quench ROS is reduced. As a result, increases in programmed cell death and reductions in population growth rate have been documented for iron- starved cells (Geider and La Roche 1994).

HNLC Phytoplankton Adaptations to Iron Limitation

Given the importance of dissolved and reduced iron to phytoplankton physiology, some phytoplankton groups have evolved adaptations to permit growth in the HNLC regions of the world's oceans. One way to reduce cellular iron quotas is to decrease cell size. The increased

surface area to volume ratio that characterizes smaller cells increases the efficiency of iron acquisition. Indeed, the observation that HNLC regions are consistently populated by phytoplankton < 5 μm (henceforth termed ultraplankton; Booth 1988; Chavez 1989) suggests that these small cells may be adapted to the iron-limiting environments of the NGA.

Another way to adapt to iron-limiting conditions is to increase acquisition of bioavailable iron. Both coastal and HNLC *Synechococcus* sp. synthesize siderophores that are released into the phycosphere, bind dissolved Fe(III), and are returned to the cell via membrane-bound transport proteins (Berube et al. 2018; Ahlgren et al. 2019). In addition to scavenging siderophore-bound iron (Kazamia et al. 2018), eukaryotic phytoplankton may also synthesize their own extracellular ligands (e.g., domoic acid produced by *Pseudo-nitzschia* spp.; Hopkinson and Morel 2009). In response to iron limitation, eukaryotic phytoplankton also increase the concentration of membrane- bound iron receptors and reductases, and/or substitute non-iron-containing proteins to carry out essential metabolic functions (McKay et al. 1999; Erdner and Anderson 1999). Conversely, Fe^{3+} receptor, and Fe^{3+} reductase production decrease in iron-replete conditions (Hudson and Morel 1990; Reid and Butler 1991), suggesting that these proteins are an evolutionary adaptation that increases phytoplankton fitness during persistent iron limitation.

Addressing the Unknowns of Iron Limitation in the NGA

Iron limitation contributes to bottom-up regulation of primary productivity in the NGA (Martin and Fitzwater 1988; Martin et al. 1989; Boyd et al. 2004). Phytoplankton community responses to iron addition result from complex interactions between iron inputs potentially differing in bioavailability and phytoplankton adaptations to HNLC conditions. The level of

complexity and high degree of variability of these interactions makes iron limitation a critical aspect of study to understand phytoplankton community structure and the productivity of the NGA. Previous deckboard incubation and *in situ* iron fertilization experiments have used synthetic $FeCl_3$ as an iron source to classify the Pacific subarctic as an HNLC ecoregion (Martin and Fitzwater 1988; Martin et al. 1989; Boyd et al. 1996, 2004). However, the bioavailability of $FeCl_3$ relative to natural sources has yet to be established. If bioavailability of $FeCl_3$ differs significantly from natural sources, previous empirical results will require reinterpretation. To address these unknowns, and to better understand factors regulating phytoplankton growth and physiology in the NGA's HNLC region, we sought to quantify the growth, community composition, and physiological responses of HNLC phytoplankton to terrigenous iron sourced via the Copper River, one of the largest point sources of iron in the NGA (Aguilar-Islas et al. 2016) compared with the synthetic source, $FeCl_3$. The primary goal of the study was to perform a 5 d grow-out iron addition experiment in which iron and macronutrient concentrations, chlorophyll *a*, community composition, and phytoplankton physiology were regularly assessed to test the following hypotheses:

1. Iron limitation is a strong bottom-up regulator of HNLC diatom growth and physiology.
    a. Cells > 20 µm exposed to $FeCl_3$ and the Copper River plume iron source will have higher net growth rates relative to the control
    b. Cells > 20 µm exposed to $FeCl_3$ and the Copper River plume iron source will have higher photosynthetic efficiency relative to the control

2. Phytoplankton < 5 μm are uniquely adapted to iron-limited conditions in the NGA HNLC region.
    a. Net growth rates for cells < 5 um will be similar for cells exposed to $FeCl_3$, Copper River plume, and control iron sources
    b. Photosynthetic efficiencies for cells < 5 um will be similar for cells exposed to $FeCl_3$, Copper River plume, and control iron sources
    c. Phycoerythrin (*Synechococcus* sp.) and chlorophyll *a* (pico- and nanoeukaryote) concentrations will be similar for cells exposed to $FeCl_3$, Copper River plume, and control iron sources
    d. Intracellular ROS concentrations will be similar for *Synechococcus* sp. and pico- and nanoeukaryotes exposed to $FeCl_3$, Copper River plume, and control iron sources
3. $FeCl_3$ will be more bioavailable to phytoplankton, relative to natural sources. Here, we define bioavailability as the ability of an iron source to improve phytoplankton physiology and increase chlorophyll *a* production efficiency.
    a. Phytoplankton net growth rates and production efficiencies (Δ chlorophyll *a*: Δ dFe) will be higher for the total phytoplankton community exposed to $FeCl_3$, relative to those exposed to the Copper River plume and control iron sources
    b. Nitrate utilization ratios (ΔN: ΔdFe) will be higher for the total phytoplankton community exposed to $FeCl_3$ than those exposed to the Copper River plume and control iron sources

Hecky and Kilham (1988) argue that deckboard iron addition experiments are speculative without ecosystem-scale corroboration. Chlorophyll *a* concentrations in bottle experiments often surpass those of *in-situ* experiments (Banse 1990; de Baar et al. 1990; Helbling et al. 1991), suggesting that no true control exists in deckboard experiments. Moreover, chlorophyll *a* accumulation can be initially similar for control and $FeCl_3$ treatments (Price et al. 1991), suggesting that bottle effects strongly influence phytoplankton response to iron addition. To address Hecky and Kilham's concerns, a secondary goal of the current study was to provide context to the iron addition experiment by characterizing phytoplankton community composition and physiology on an ecosystem scale. We, therefore, separately sampled the ambient phytoplankton communities along three transects in the summer of 2019 (Figure 1) to quantify chlorophyll *a* biomass, photosynthetic efficiency, and the abundance and physiology of cells < 5 µm. Given strong cross-shelf gradients in phytoplankton community composition and physiology observed in the NGA, sampling these transects provided a wide range of natural responses to which the phytoplankton responses in our iron addition experiment were compared.

METHODS

Study Site

To investigate the growth and physiology of HNLC phytoplankton exposed to different sources of iron-rich seawater, a 5 d deckboard incubation experiment was performed aboard the *R/V Sikuliaq* in conjunction with the NGA Long-Term Ecological Research (LTER) program. The NGA LTER study site is composed of three transects, including the historically sampled Seward Line, and extends southwestward from Middleton Island west of the Copper River to Kodiak Island (Figure 1). The site covers an area approximately 2.2 x 10^5 km^2 in size. Though the Seward Line has been episodically sampled since the 1970s and systematically since 1998 (Janout et al. 2010), sampling of the additional LTER transects started in Spring of 2018. The following iron addition experiment and associated environmental sampling was conducted during a process cruise from 25 June to 15 July 2019.

Water Collection

The iron addition experiment utilized near-surface seawater (~ 1.5 m) collected from two distinct regions of the NGA: The Copper River plume and the HNLC region. Water was collected from the Copper River plume near 60° 11.49’ N, 145° 33.00’ W on 04 July 2019. The HNLC sampling site was identified prior to sampling using the *R/V Sikuliaq* under-way system (Nitrate ~ 3.5 µM; Salinity ~ 32.2 psu) and sampled near 57° 21.05’ N, 145° 42.80’ W on 08 July 2019. Water was collected using a trace-metal-clean pumping system consisting of Teflon™ tubing attached to the outside of a bathythermograph towed 5 m away from the side of the ship to avoid contamination from the ship (Bruland et al. 2005; Aguilar-Islas and Bruland 2006). Water

was filtered in-line through a 0.2 µm Supor filter capsule (AcroPak™ 200) to remove all particles. In addition to the two filtered seawater (FSW) sources, an additional unfiltered sample from the HNLC site was collected and gently pre-screened through a 200 µm Nitex mesh to remove large zooplankton. This water, containing the intact HNLC community < 200 µm and referred to hereafter as $HNLC_{200}$, served as the source of HNLC phytoplankton. All water samples were stored in acid-washed, low-density polyethylene carboys in darkness at 13 °C until use in the experiment.

Experimental Setup

The experimental setup is diagrammed in Figure 2. All experimental processing was carried out under positive pressure inside a plastic enclosure built inside the ship using trace metal clean techniques. Three treatments were created by mixing FSW 1:3 with $HNLC_{200}$ in separate acid-washed carboys (referred to hereafter as "mixed carboys"). A 1:3 FSW: $HNLC_{200}$ ratio was chosen to reduce dilution of the HNLC phytoplankton community and to maintain a salinity ~ 32.2 psu in experimental bottles. For the control treatment, a mixture of 8 L HNLC FSW and 17 L $HNLC_{200}$ was created and dispensed into ten 2.3 L polycarbonate bottles. To allow comparisons of natural iron sources to sources used in previous iron addition experiments in the NGA, another HNLC FSW:$HNLC_{200}$ mixture was combined in a 1:3 ratio and spiked with $FeCl_3$ to a final Fe concentration of 4.56 nM. This mixture constituted the "$FeCl_3$" treatment and was used to fill an additional ten 2.3 L polycarbonate bottles. To prepare the "river plume" treatment, 7.0 L of Copper River plume FSW was first diluted with 1.0 L of HNLC FSW to maintain a salinity of ~ 27 psu in the Copper River plume FSW:$HNLC_{200}$ mixture and limit changes in HNLC phytoplankton physiology due to salinity stress. Seventeen liters of $HNLC_{200}$

was then added to this diluted Copper River FSW. This combined mixture constituted the "river plume" treatment and was used to fill a final ten 2.3 L polycarbonate bottles.

To avoid iron contamination during the incubation period, each replicate bottle (N= 30) was capped, sealed with Parafilm and electrical tape and placed in two plastic Ziploc® bags tightly secured using electrical tape. Filled bottles were stored in darkness at 13 °C until all treatments were mixed and all replicate bottles filled.

Incubation and Sampling- Replicate bottles were incubated on-deck over the course of five days in two plexiglass incubators. Placement of replicate bottles within incubators was haphazard. Incubation temperature was maintained using an under-way flow through system and averaged 14.5 ± 0.1 °C throughout the experiment. Photosynthetically active radiation (PAR) was controlled to the 50 % ambient light level using a single layer of neutral density screen around each bottle. A Li-Cor 2π quantum sensor secured to the ship's superstructure collected incident PAR data.

Experimental bottles from each treatment were sacrificially sampled at regular intervals to quantify phytoplankton biomass, community composition, physiology, and nutrient use. Initial bottles (n= 1) were sampled immediately after the start of incubation at 21:30 on 08 July 2020. Two bottles per treatment were sampled at 48 h, 72 h, and 96 h, while three bottles per treatment were sampled at 120 h. This unbalanced experimental design represented a compromise between the logistic feasibility of performing a large iron addition experiment and the desire to replicate measurements at each time point. Specific sampling techniques are described in further detail below.

Size-fractionated Chlorophyll a and Fv/Fm

Chlorophyll *a* concentrations were obtained for phytoplankton > 20 µm, 5- 20 µm, and < 5 µm and used as a proxy for biomass. 75 mL aliquots were vacuum-filtered in parallel through 20- and 5 µm (25 mm) PCTE filters (Thomas Scientific) and a 0.7 µm (25 mm) glass fiber filter (VWR International). Pigments were then extracted in 90 % acetone over 24 h (dark; -20 °C) and red autofluorescence was measured on a Turner 10-AU fluorometer following the acidification method of Holm-Hansen et al. (1965).

Size-fractionated and total community measurements of photosynthetic efficiency (Fv/Fm) were used as an indicator of photosystem II stress (Krause and Weis 1984; Greene et al. 1992). 50 mL aliquots were gravity-filtered through 20- and 5 µm (25 mm) PCTE filters (Thomas Scientific). Cells were then resuspended from the 20 µm filter into 25 mL of FSW following Cermeño et al. (2005) to isolate cells > 20 µm. Filtrate from the 5 µm filter was collected and used to determine the Fv/Fm of phytoplankton < 5 µm. 5 mL subsamples (in triplicate) were taken from the resuspension, the filtrate, and the incubation bottle (to characterize the total community). All subsamples were dark acclimated at ~ 13 °C for 20 min (as determined by preliminary tests; data not shown) before Fv/Fm was measured on a WALZ Water-PAM fluorometer (Alderkamp et al. 2010).

Flow Cytometric Analysis of Phytoplankton < 20 µm

Two types of flow cytometry samples were used to characterize the physiology and abundance of *Synechococcus* sp. and pico- and nanoeukaryotes. “Community composition” samples (2.0 mL, in duplicate) were filtered through a 20 µm (25 mm) PCTE filter (Thomas

Scientific) and used to quantify cell abundance and qualitatively assess cell size and photosynthetic pigment content (Dubelaar and Jonker 2000).

Oxidative stress was qualitatively assessed with the CellROX™ Green intracellular probe (Cheloni et al. 2014). The probe was obtained from ThermoFisher Scientific and prepared by diluting 50 µL aliquots of CellROX™ Green in 150 µL of pre-filtered (0.2 µm) DMSO. To prevent degradation of the probe, it was stored in darkness at – 20 °C until use in the experiment. Duplicate "ROS" samples (1.0 mL), pre-filtered through a 20 µm filter, were treated with CellROX™ Green to a final concentration of 5 µM. All flow cytometry samples were dark-incubated for 60 minutes at 13 °C before being fixed with pre-filtered (0.2 µm) paraformaldehyde (0.5 % v/v) and flash frozen in liquid nitrogen. Samples were stored in darkness at – 80 °C for flow cytometric analysis onshore.

Samples were thawed immediately before they were run on a Becton-Dickson FACSCalibur equipped with a 15 mW 488 nm argon laser. Each flow cytometry sample was run twice in succession at a medium flow rate for 120 s. Prior to running samples on the flow cytometer, a bead solution of known concentration (4.12×10^5 beads mL^{-1}) was made using Yellow-Green Fluoresbrite® microspheres (1 µm, Polysciences Inc.). A 50 µL aliquot of this bead solution was added to each flow cytometry sample. The inclusion of beads in each sample served as an internal standard to normalize fluorescence properties and was used to establish analysis volumes for each flow cytometry run (Dubelaar and Jonker 2000; Collier and Palenik 2003). Analysis volumes were calculated as the number of beads detected, relative to the concentration of beads in each sample. *Synechococcus* sp. and pico- and nanoeukaryote abundances were then calculated based on the analysis volume of each run.

Listmode files (FSC 2.0 format) containing forward light scatter (FSC), red (FL3) and orange (FL2) autofluorescence, and green fluorescence (FL1) for each event recorded by the flow cytometer were acquired using CellQuest Pro (Table 1). FlowJo (v. 10; BD Life Sciences) was used to import FSC files and visually gate *Synechococcus* sp. and pico- and nanoeukaryote populations (Figure S1). To avoid the inclusion of debris particles and cell aggregates in data analysis, *Synechococcus* sp. and pico- and nanoeukaryote populations were further refined by analyzing relative frequency distributions of FSC (bin width 2 and 10, respectively). Particles in bins with a relative frequency of < 5 % were identified as outliers and eliminated from *Synechococcus* sp. and pico- and nanoeukaryote population estimates. Microscopy based estimates at 0 h and 120 h of the iron addition experiment and a subset of LTER transect stations suggested that flow cytometry under-estimated *Synechococcus* sp. abundance. Underestimation of *Synechococcus* sp. was likely due to clumping of cells and the removal of these aggregates from the *Synechococcus* sp. population. We determined that the average offset for *Synechococcus* sp. in the iron addition experiment and LTER transect stations was 44 % and 33 %, respectively (e.g., Figure S2), and counts were adjusted accordingly. Once *Synechococcus* sp. and pico- and nanoeukaryote populations were refined, FL1, FL2, and FL3 for each cell in each run were normalized to the *median* of the respective bead parameter.

Levels of green fluorescence observed in "ROS" samples derive from two major sources: endogenous green fluorescence after aldehyde fixation (Vaulot et al. 1989) and the activation of the CellROX™ Green probe by metabolic production of intracellular ROS (Salin 1988). To control for background (i.e. endogenous) levels of green fluorescence, the bead-normalized FL1 signal of each *Synechococcus* sp. and pico- and nanoeukaryote cell in "probed" ROS samples was normalized again to the *mean* bead-normalized FL1 signal for the corresponding population

in “un-probed” community composition samples. The normalized FL1 ratio for a given cell is given by Equation (1).

$$FL1\ ratio_{Cell\ \ in\ ROS\ sample} = \frac{Bead\ Normalized\ FL1_{\ Cell\ in\ ROS\ sample}}{mean\ (Bead\ Normalized\ FL1_{Cells\ in\ Comm.\ Comp.\ sample})} \quad (1)$$

If ROS production decreases with the addition of iron, the FL1 ratio should be lower in the river plume and iron chloride treatments, relative to the control.

Microscopic Analysis of Diatom Community Composition

To quantify changes in the diatom community composition during the incubation, 250 mL samples were fixed with 4.4 mL borate-buffered formalin at the initial (0 h) and final (120 h) time points. Samples were settled using the Utermöhl method (Lund et al. 1958) for ≥ 12 h before diatoms were enumerated under inverted microscopy (magnification 125X and 250X). Diatoms were identified at the genus level, enumerated, and measured using a digitizing system and the MicroBiota program (Roff and Hopcroft 1986). Since a 2D focal plane restricted the ability to measure diatom depth, Microbiota utilized a taxa-specific depth assumption, defined as a fraction of cell width, to estimate the depth of each cell measured. Estimates of biovolume for each diatom cell were delivered by Microbiota based on the relationship between depth assumption and taxa-specific shape (Table S1). Biovolumes were then converted to biomass estimates using a C: volume relationship for diatoms established by Menden-Deuer and Lessard (2000). Diatom biomass estimates were partitioned by taxon to assess changes in diatom community composition across treatments and aggregated to obtain total diatom biomass for each treatment.

Nutrient Analysis

All nutrient samples were collected by Dr. Ana Aguilar-Islas and analyzed at the University of Alaska-Fairbanks in the Nutrient Analytical Facility. Macronutrient (nitrate, nitrite, phosphate, and silicic acid) analyses were performed on a Seal Analytical continuous-flow QuAAtro39 AutoAnalyzer using methods derived from Armstrong et al. (1967; nitrate, nitrite, silicic acid) and Murphy and Riley (1962; phosphate). Micronutrient (e.g., dissolved Fe (dFe) and dissolved Copper (dCu)) concentrations were measured following protocols outlined in Aguilar-Islas et al. (2016).

Contextualizing the Iron Addition Experiment

To provide environmental context to the iron addition experiment, phytoplankton communities in the iron addition experiment were compared to ambient phytoplankton communities at 23 stations along three LTER transects (Figure 1). Surface water (< 4 m depth) was obtained from Niskin bottles on a Seabird SBE 9/11 Plus CTD at each station sampled. Water for flow cytometry samples was filtered in-line through a 50 µm mesh. Measurements of size-fractionated chlorophyll *a*, Fv/Fm (Total, < 5 µm, and > 5 µm), and flow cytometric properties (including intracellular ROS content) for *Synechococcus* sp. and pico- and nanoeukaryotes were obtained using methods described above.

Data Analysis

All statistical analyses were performed in R (v. 3.6.2). Given the variability in natural phytoplankton communities, the inability to distinguish the majority of phytoplankton species,

and divergent growth in replicate bottles, alpha was set to 0.10 for all statistical analyses unless otherwise noted.

Net growth rates for phytoplankton were derived from the ordinary least squares regression coefficients of ln-transformed chlorophyll *a* versus time for 48 h -96 h. Differences in net growth rates across treatments were determined using Tukey's pairwise contrasts.

Differences in size fractionated Fv/Fm and in *Synechococcus* sp. and pico- and nanoeukaryote flow cytometric measurements across treatment and time were determined using a full or reduced Generalized Least Squares Model (Equation 2). Where treatment: time interaction was not significant, a reduced model was used (see below). In cases where the treatment:time interaction was significant, Tukey's pairwise contrasts were used to compare *slopes* across treatment.

$$Y = \beta_0 + \beta_1(Treatment) + \beta_2\,(Time) + \beta_3(Treatment)(Time) + \varepsilon \qquad (2)$$

In cases where no significant treatment:time interaction was observed, a reduced GLS model (Equation 3), followed by Tukey's pairwise contrasts, was used to test differences across treatment *means*.

$$Y = \beta_0 + \beta_1\,(Treatment) + \beta_2\,(Time) + \varepsilon \qquad (3)$$

In all cases, models were visually validated by plotting residuals and checking for normality and homoscedasticity. The residuals for pico- and nanoeukaryote abundance were not normally

distributed, and this variable was analyzed using a Generalized Linear Mixed Model (*nlme* package) that accounted for flow cytometer run, replicate, and experimental bottle.

A multiple algorithm approach, combining Ward's hierarchical classification on principal components and K-means aggregation, was used to contextualize the phytoplankton communities in the iron addition experiment within the ambient communities sampled on the NGA transects (Ben-Hur and Guyon 2003; Argüelles et al. 2014). Total chlorophyll *a* and Fv/Fm measurements were highly correlated with size-fractioned values (Pearson's r = 0.91 and 0.92, respectively). Therefore, only chlorophyll *a* and Fv/Fm measurements for the total phytoplankton community, along with all flow cytometric measurements for *Synechococcus* sp. and pico- and nanoeukaryotes, for each iron treatment or station were used in principal components analysis. A scaled and centered principal components analysis was run using the *prcomp* function in R. Euclidean distance and Ward's minimum variance method were then used to cluster the first 8 (of 10) principal components.[1]

After the hierarchical clustering of principal components was performed, K-means aggregation was used to identify regional groupings. Optimization of K-means mobile centers was performed using the "elbow" method (Bholowalia and Kumar 2014; Yuan and Yang 2019) and indicated clusters could be split into three regional groups. This multiple algorithm method generated a dendrogram with clusters containing both iron addition and LTER transect samples nested within three robust regional groups.

[1] Ben-Hur and Guyon (2003) recommend using the minimum number of principal components that generate stable clusters in the final dendrogram presented in publication. Preliminary clustering analysis of principal components (data not shown) indicated that the inclusion of 8 components met this requirement.

RESULTS

Growth and Physiology of the Total Phytoplankton Community

The NGA HNLC phytoplankton community responded differentially to the iron treatments. After a 48-h lag, total chlorophyll *a* biomass increased rapidly in the $FeCl_3$ treatment (specific net growth rate = 0.78 d^{-1}) and more slowly in the river plume (0.47 d^{-1}) and control treatments (0.31 d^{-1}; Table 2). Total chlorophyll *a* peaked at 2.82 $\pm$ 0.12 µg L^{-1} (mean $\pm$ 1 sd) for cells exposed to $FeCl_3$ at 96 h before leveling off (Figure 3A). Leveling off of total chlorophyll *a* biomass occurred only in the $FeCl_3$ treatment after 96 h and coincided with near exhaustion of nitrate and silicic acid (Figures 4A, 4D).

The addition of the $FeCl_3$ and river plume iron sources increased photosynthetic efficiency for the total phytoplankton community. Average Fv/Fm for the total phytoplankton community ranged from 0.40 $\pm$ 0.01 to 0.53 $\pm$ 0.01 and was consistently highest in the $FeCl_3$ treatment (Figure 5A; Table 3). With the exception of a slight decrease from 0 h – 48 h in the control, Fv/Fm remained consistent over the duration of the experiment and averaged 0.40 $\pm$ 0.04, 0.49 $\pm$ 0.02, and 0.53 $\pm$ 0.04 in control, river plume, and $FeCl_3$ treatment, respectively (Table 3). The response of phytoplankton > 20 µm mirrored that of the total community, responding uniquely to each of the three iron sources, while cells < 20 µm responded similarly to the river plume and $FeCl_3$

Growth and Physiology of Cells > 20 µm

The addition of $FeCl_3$ stimulated a diatom bloom, indicated by an increase in the chlorophyll *a* > 20 µm concentrations (Figure 3D) and the fraction of total chlorophyll *a* > 20

μm (Figure 3E), that was less pronounced in the control and river plume treatments. Net growth rates of cells > 20 μm were ≥ 2X higher in the $FeCl_3$ treatment than in the control and river plume treatments (Table 2). Though control and $FeCl_3$ treatments contained the same dominant diatom species, diatom biomass ($z = 2.66$, $p= 0.022$) and abundances ($z= 11.49$, $p < 0.0001$) were higher in the $FeCl_3$ treatment at the end of the experiment (Figures 6, 7). The pennate diatom *Pseudo-nitzschia* spp. (e.g. *P. multiseries*, *P. delicatissima*, and *P. pungens*) and centric diatom *Thalassiosira* spp. (e.g. *T. pacifica*, *T. eccentrica*, and *T. nordenskioeldii*) dominated the diatom community in these two treatments and together comprised over 92 % of total cells (Figure 7) and 45 % of total diatom biomass (Figure 6).

In contrast to the $FeCl_3$ treatment, the river plume treatment produced only marginally more chlorophyll *a* > 20 μm and diatom biomass ($z= 0.88$, $p= 0.66$) than the control (Figures 3D, 6). However, increased drawdown of dFe in the first 48 hours (Figure 8A) and higher chlorophyll *a* > 20 μm biomass in the river plume treatment (Figure 3D) suggest that the iron in the river plume treatment was more bioavailable than that in the control. *Pseudo-nitzschia* spp. and *Thalassiosira* spp. were present in the river plume treatment at much lower concentrations than those observed in the control or $FeCl_3$ treatments and constituted only ~ 21 % of total diatom biomass (Figure 6). Small chain-forming *Rhizosolenia* spp. (comprised of cells < 100 μm in length), rarely observed in the control and $FeCl_3$ treatment, averaged $4.78 \times 10^4 \pm 3.26 \times 10^4$ cells L^{-1} in the river plume treatment. These cells comprised ~ 30 % of total diatom abundance (Figure 7) and almost 13 % of total diatom biomass. Large *Rhizosolenia* spp. (single cells > 100 μm in length) were also more abundant in the river plume treatment than in the control and $FeCl_3$ treatments and constituted nearly 30 % of total diatom biomass (Figure 6). In all treatments, a

mixture of dominant chain-forming species and a minority of large, single-celled species constituted total diatom biomass (Tables S2, S3).

Photosynthetic efficiency for cells > 20 µm was consistently highest in the $FeCl_3$ treatment, intermediate in the river plume treatment, and lowest in the control (Table 3). Fv/Fm was elevated in the $FeCl_3$ treatment even at 0 h, indicating a rapid response to $FeCl_3$ addition during experimental setup. After 0 h, Fv/Fm for cells > 20 µm diverged in all treatments, remaining low in the control. A precipitous decrease in Fv/Fm from 0.45 ± 0.10 to 0.08 ± 0.04 occurred in the control phytoplankton community in the first 48 h. After 48 h, the Fv/Fm of the control phytoplankton community increased, averaging 0.28 ± 0.06 for the remainder of the experiment (Figure 5C). Despite similar total diatom biomass in the control and river plume treatments, Fv/Fm was elevated in the river plume treatment, further supporting differential bioavailability of this iron source.

Growth and Physiology of Cells < 20 µm

In contrast to diatoms, which showed differential community composition and physiological responses to all three iron sources, the response of phytoplankton < 20 µm suggested that some of these cells responded similarly to the river plume and $FeCl_3$ iron sources. Net growth rates from chlorophyll *a* were lowest for cells < 5 µm, reaching only 0.15 d^{-1}, 0.39 d^{-1}, and 0.55 d^{-1} for the control, river plume, and $FeCl_3$ treatments, respectively (Table 2). Chlorophyll *a* < 5 µm was highest in the $FeCl_3$ treatment and diverged from the control after 48 h (Figure 3B). Net growth rates for cells 5- 20 µm were higher than those of the smallest cells, reaching 0.53 d^{-1}, 0.66 d^{-1}, and 0.71 d^{-1} in the control, river plume, and $FeCl_3$ treatments,

respectively (Table 2). Chlorophyll *a* in the 5- 20 µm size fraction was highly variable but closely mirrored that of cells < 5 µm (Figure 3C).

Both the river plume and $FeCl_3$ iron sources increased *Synechococcus* sp. abundance similarly, relative to the control. *Synechococcus* sp. abundance increased rapidly in all treatments for the first 72 h before growth tapered in the control (Figure 9A). *Synechococcus* sp. abundance was higher in the river plume and $FeCl_3$ treatments than in the control after 48 h and increased at an average rate of 2,165 and 2,101 cells d^{-1}, respectively. At the end of the experiment, *Synechococcus* sp. abundances in the river plume and $FeCl_3$ treatments were nearly identical, reaching 2X those of the control (Figure 9A; Table 4).

The addition of the $FeCl_3$ and river plume iron sources enabled *Synechococcus* sp. cells to increase in size, relative to the control. On average, cells were largest in the $FeCl_3$ treatment and intermediate in the river plume treatment. *Synechococcus* sp. FSC increased throughout the experiment for *Synechococcus* sp. in the river plume and $FeCl_3$ treatments at equal rates (Table 4) but remained nearly constant in the control (Figure 9B).

Pico- and nanoeukaryote abundance remained constant in all treatments within the first 72 h, averaging 67,000 $\pm$ 3,200 cells mL^{-1} (Figure 10A) before decreasing precipitously. After 72 h, concentrations decreased at equal rates in all treatments (Table 4). Final pico- and nanoeukaryote abundances ranged from 46,000 cells mL^{-1} to 53,000 cells mL^{-1}, representing a ~ 25 % decrease in pico- and nanoeukaryote abundance in all treatments.

As with *Synechococcus* sp., pico- and nanoeukaryotes were largest, on average, in the $FeCl_3$ and river plume treatments. Average pico- and nanoeukaryote FSC increased rapidly in all treatments during the first 48 h. After 48 h, treatments diverged, with pico- and nanoeukaryotes

in the river plume and $FeCl_3$ treatments becoming larger than those in the control treatment (Figure 10B, Table 4).

The $FeCl_3$ and river plume iron sources increased photosynthetic pigment content, relative to the control, and did so to equal extents for both *Synechococcus* sp. and pico- and nanoeukaryote cells. Phycoerythrin content per cell (FL2) increased in all treatments throughout the experiment but remained similar between the river plume and $FeCl_3$ treatments (Figure 9C, Table 4). *Synechococcus* sp. chlorophyll *a* content was also highest in the $FeCl_3$ and river plume treatments (Figure 9D). Trends in pico- and nanoeukaryote chlorophyll *a* content closely matched those of *Synechococcus* sp., with average chlorophyll *a* per cell (FL3) remaining nearly identical in the $FeCl_3$ and river plume treatments, but higher than in the control (Figure 10C, Table 4). In contrast to *Synechococcus* sp. which did not exhibit an ROS response (Figure 9E, Table 4), intracellular ROS concentrations (FL1 ratio) for pico- and nanoeukaryotes were highest in the control (with the exception of the 72 h time point), intermediate in the river plume treatment, and lowest in the $FeCl_3$ treatment (Figure 10D, Table 4).

Fv/Fm values remained nearly identical between the river plume and $FeCl_3$ treatments for cells < 5 µm, yet Fv/Fm in both treatments were consistently higher than in the control (Figure 5B, Table 3). Fv/Fm decreased during the first 48 h for the control treatment, reaching a minimum of 0.31 ± 0.01 before gradually increasing to 0.41 ± 0.01 by 96 h.

Macro- and Micronutrient Dynamics

Macronutrient (nitrite, nitrate, phosphate, and silicic acid) drawdown was commensurate with diatom growth in all treatments (Figure 4). The addition of the river plume water to the HNLC sample nearly doubled initial Si concentrations while decreasing the available N and P.

However, N and P concentrations at 0 h were well above limiting levels for phytoplankton in all treatments. Throughout the incubation, drawdown of silicic acid was observed in the river plume and $FeCl_3$ treatments and was accompanied by slower drawdown of nitrate. $Si(OH)_4$:N utilization ratios remained well above the expected 1:1 ratio in the river plume and $FeCl_3$ treatments (Table 5). Residual $Si(OH)_4$ at 120 h after N depletion, coupled with increasing N:P ratios (Table S4) in control and $FeCl_3$ treatments indicate that diatom growth was likely N-limited by the end of the experiment.

Dissolved iron drawdown was also commensurate with phytoplankton growth in all treatments. Dissolved iron was ~ 3.5 nM higher in the $FeCl_3$ treatment, relative to the river plume treatment and control at 0 h (Figure 8). Maximum dFe drawdown occurred in all treatments within the first 48 h and was steepest in the $FeCl_3$ treatment. dFe concentrations were highest in the $FeCl_3$ treatment throughout the entire incubation but were indistinguishable between the control and river plume treatments from 48 h – 120 h (Figure 8). Nitrate utilization ratios and total phytoplankton chlorophyll *a* production efficiencies, with respect to dFe, were ~ 2.5X and ~ 1.5X higher in the river plume treatment, respectively, than in either the control or $FeCl_3$ treatment (Table 5).

Contextualizing the Iron Addition Experiment

During the summer of 2019, total chlorophyll *a* biomass in surface waters of the NGA remained low (< 2.0 µg L^{-1}) on all three transects and, like the communities in the control and river plume treatments, was dominated by cells < 5 µm. Total chlorophyll *a* biomass in the control and river plume treatments at 120 h fall well within the range measured in ambient

phytoplankton communities, while chlorophyll *a* biomass in the $FeCl_3$ treatment (2.74 µg L^{-1}) slightly exceeded the highest levels observed in the NGA (Figure 11).

Elevated chlorophyll *a* concentrations were observed at select stations and often coincided with suspected sources of iron. Chlorophyll *a* concentrations > 1.0 µg L^{-1} were observed at both MID 6 and KOD 5. These stations are among the shallowest on the shelf (~ 60 m depth) and subsurface iron is likely sourced to surface waters by intense tidal mixing. Elevated chlorophyll *a* > 20 µm was also observed in eddy- influenced waters at the end of the MID Line, at GAK 15, at KOD 5, and in the center of a mesoscale eddy (EATJ) sampled at the end of the KOD Line ~ 200 nmi offshore (Figure 11). Though chlorophyll *a* > 20 µm was elevated at these discrete sites, chlorophyll *a* > 20 um constituted a maximum of 24 % of total chlorophyll *a* biomass.

Total photosynthetic efficiencies measured in the iron addition experiment agreed well with ambient phytoplankton communities on NGA transects. Total photosynthetic efficiency for communities on the MID and KOD lines remained consistently high (> 0.4) and was similar to total Fv/Fm in the river plume and $FeCl_3$ treatments of the iron addition experiment (Figure 12). In contrast to the high Fv/Fm values observed on the MID and KOD lines, total Fv/Fm for ambient phytoplankton communities on the GAK line decreased across the shelf (Figure 12A). Phytoplankton offshore at GAK 15 had photosynthetic efficiencies approaching 0.2 and were most similar to the control in the iron addition experiment, which averaged 0.35. Fv/Fm < 5 µm (Figure 12B) tracked total Fv/Fm closely, while Fv/Fm > 5 µm (Figure 12C) was more variable and ranged from 0.13 to 0.60.

Nano- and picoeukaryote abundances, cell size, and chlorophyll *a* content were similar between ambient communities and those in the iron addition experiment at 120 h. Pico- and

nanoeukaryote abundances in ambient communities averaged 5.1 x 10^4 ± 1.2 x 10^5 cells mL^{-1} (mean ± range) and were lowest on the middle of the KOD Line (Figure 13A). In contrast to the low abundances of pico- and nanoeukaryotes observed on the KOD Line, pico- and nanoeukaryotes bloomed on the inner MID Line and at GAK 5. Abundances at 120 h in the iron addition experiments closely matched those of ambient communities on all transects and were particularly similar to communities sampled at the beginning of the MID Line (Figure 13A). Pico- and nanoeukaryotes were largest on the GAK line and averaged 39.82 ± 21.78 (mean ± range) across all transects (Figure 13B). Though pico- and nanoeukaryotes at 120 h in the iron addition experiment were larger, on average, than those observed in the ambient community, FSC of these cells fell within the range of the natural communities observed in the NGA. Chlorophyll *a* content for pico- and nanoeukaryotes peaked on the middle of all three LTER transects (Figure 13C) and agreed with chlorophyll *a* content observed for cells in the iron addition experiment at all stations sampled. Nano- and picoeukaryote FL1 ratios were similar for communities on all three transects and averaged 1.81 ± 0.73 across the shelf. ROS content was elevated for *in situ* nano- and picoeukaryote cells, relative to cells in the iron addition treatment (Figure 13D).

In contrast to the pico- and nanoeukaryotes, *Synechococcus* sp. in the iron addition experiment did not agree as well with ambient communities. *Synechococcus* sp. abundance averaged 1.1 x 10^5 ± 3.1 x 10^5 cells mL^{-1} across all transects and was notably highest on the MID Line (Figure 14A). While *Synechococcus* sp. abundances were, on average, 1-2 orders of magnitude higher in ambient communities than in the iron addition experiment, low abundances at the end of the GAK Line (i.e., GAK 11 and GAK 13) were similar to final *Synechococcus* sp. abundances in the river plume and $FeCl_3$ treatments (Figure 14A). *Synechococcus* sp. were

largest in the coastal waters on the GAK Line; cell size decreased in offshore waters on the GAK and MID Lines (Figure 14B). *Synechococcus* sp. *in situ* remained smaller, on average, than cells measured in the river plume and $FeCl_3$ treatments of the iron addition experiment (Figure 14B). Phycoerythrin content (FL2) in ambient *Synechococcus* sp. communities averaged 0.31 ± 1.19 (mean $\pm$ range) across all transects (Figure 14C) and was consistently highest on the KOD Line. FL2 was similar for *Synechococcus* sp. in ambient phytoplankton communities and cells measured in the iron addition experiment. FL1 ratios for *Synechococcus* sp. cells was highly variable across transects but was generally highest on the inner MID Line (Figure 14D). ROS content for *Synechococcus* sp. in our experiment was lower, on average, than that of the ambient communities in the NGA.

Multivariate clustering of LTER and iron addition experiments resulted in nested groups of samples in three distinct regions based on similarity (Figure 15). As expected, initial phytoplankton communities in each experimental treatment clustered tightly together and were most similar to potentially Fe-limited offshore stations (GAK 11, GAK 15, EATJ, and MID 10) and one mid-shelf station (GAK 5; Figure 15). Phytoplankton communities in the control remained clustered with offshore stations at 120 h, while those of the river plume and $FeCl_3$ treatments were most similar to stations on the mid- and inner shelf (e.g., KOD 5, KOD 9, MID 6). These stations were among the most productive sampled in the NGA, with chlorophyll *a* biomass ranging from 0.51- 1.64 μg L^{-1} and Fv/Fm ranging from 0.44- 0.59.

While ambient phytoplankton communities in the NGA and those of the iron addition experiment clustered predictably, ROS content of pico- and nanoeukaryotes in the control treatment was generally higher than on LTER transects and was similar to ambient communities with Fv/Fm ≤ 0.4. In contrast, ROS content of *Synechococcus* sp. were generally lower than

communities on LTER transects. These results suggest that pico- and nanoeukaryotes were more stressed- and *Synechococcus* sp. less stressed- in the control of our experiment than *in situ*.

DISCUSSION

Overview

Though iron limitation of phytoplankton in HNLC regions is well established (Martin and Fitzwater 1988; Behrenfeld et al. 1996; Boyd et al. 2004), we are among the first to directly compare the bioavailability of natural and synthetic iron sources. Our study yields several insights regarding the bioavailability of iron to the NGA HNLC phytoplankton community. Firstly, the physiological response of phytoplankton > 20 µm to $FeCl_3$ addition aligns well with previous iron addition experiments and confirms that NGA diatom biomass is regulated by iron limitation in offshore waters. Secondly, shifts in diatom physiology and community composition indicate that the $FeCl_3$, the control, and river plume iron sources represent distinct pools of iron, each differing in bioavailability to phytoplankton > 20 µm. Thirdly, despite the proposed benefits of increased surface area:volume ratios, the physiological response of pico- and nanoeukaryotes to iron addition indicates that these cells were stressed by low iron availability *in situ*. Finally, differences in nutrient use and chlorophyll *a* production efficiencies for total phytoplankton communities highlight divergent ecological fates of the $FeCl_3$ and the river plume iron sources. We urge the re-interpretation of previous iron addition experiments utilizing $FeCl_3$ to model diatom growth and highlight the importance of fluvial iron input in maintaining HNLC ultraplankton communities.

Growth and Physiology of Cells > 20 µm

All physiological indicators confirm that iron addition from either source alleviated iron stress for cells > 20 µm (Table 6). Iron concentrations were elevated in the HNLC

FSW:$HNLC_{200}$ carboy (0.8 nM) compared to the ambient HNLC water (0.08 nM), indicating contamination of the control treatment during collection or subsampling by an unknown iron source. This contamination resulted in initial control dFe concentrations nearly matching those of the river plume treatment (~ 1 nM). Despite similar concentrations of initial dFe in these two treatments, increased net growth rates and photosynthetic efficiency in the river plume treatment indicate that fluvial iron input can reduce photo-oxidative stress in cells > 20 µm. These observations suggest that the fluvial iron source is more bioavailable than the HNLC source.

Fv/Fm between the $FeCl_3$ and control treatments differed at 0 h, indicating a rapid increase in photosynthetic efficiency (< 5 h response time) with the introduction of $FeCl_3$ during experimental setup. Immediate increases (< 6 h response time) in photosynthetic efficiency in response to $FeCl_3$ addition have been documented for *Pseudo-nitzschia* spp. in culture (Marchetti et al. 2009) and for the total phytoplankton community in the IronEx II fertilization experiment performed in the equatorial Pacific (Behrenfeld et al. 1996). When considering the range of Fv/Fm measurements taken in iron fertilization experiments around the globe (0.3 – 0.65), the photosynthetic efficiency of cells > 20 µm in our $FeCl_3$ treatment approaches the theoretical maximum for diatoms (Suzuki et al. 2009). High photosynthetic efficiency of diatoms, coupled with net growth rates approaching theoretical maxima for diatoms at 10 °C (Eppley 1972; Boyd et al. 1996), not only indicate that $FeCl_3$ is more bioavailable than the HNLC and river plume iron sources, but also confirm iron limitation as a bottom-up regulator of large-celled phytoplankton in the offshore NGA.

Decreased abundance of *Pseudo-nitzschia* spp. in the river plume treatment reflects differential bioavailability of the river plume and $FeCl_3$ iron sources and is notable, given that *Pseudo-nitzschia* spp. dominated diatom blooms in multiple iron addition experiments

(Cavender-Bares et al. 1999; Landry et al. 2000a; b; Assmy 2004; Boyd et al. 2007; Marchetti et al. 2009). There are several non-mutually exclusive hypotheses that may explain decreased *Pseudo-nitzschia* sp. abundance in the river plume treatment. Salinity stress may have inhibited the growth of *Pseudo-nitzschia* spp. in the river plume treatment, although we believe this is unlikely given that *P. multiseries*, *P. delicatissima*, and *P. pungens* are globally distributed (Trainer et al. 2012) and that *Pseudo-nitzschia* spp. grow well at salinities ranging from 15 – 40 psu (Lundholm et al. 1997; Thessen et al. 2005).

Trace metal toxicity may have also reduced *Pseudo-nitzschia* spp. growth in the river plume treatment, where total dissolved copper was twice as high as in other treatments (Figure 8B). The detrimental effects of high copper concentration on phytoplankton growth and physiology are well established (Brand; Sunda 1975); however, we measured total dissolved copper, and do not know the concentration of inorganic copper, the toxic copper species. Nonetheless, even if a large fraction of the total dissolved copper in the river plume treatment was inorganic copper, diatoms appear to be resistant to copper at ambient concentrations exceeding those observed in our experiment (i.e., 3.9 nM; Brand 1986; Coale 1991). Moreover, comparative studies of *Pseudo-nitzschia* spp. demonstrate that both *P. multiseries* and *P. delicatissima* grow well at copper concentrations < 96 µg L^{-1} (~ 1500 nM; Lelong et al. 2012, 2013), possibly due to the use of copper in iron acquisition systems (Rue and Bruland 2001; see below). While the toxicity of other trace metals (or deleterious synergies between copper and other trace metals) cannot be eliminated, it is unlikely that dissolved copper concentrations ~ 3 nM alone inhibited *Pseudo-nitzschia* spp. growth in our experiment.

Top-down regulation of diatom communities has been observed in a few iron addition experiments (Landry et al. 2000a; b; Coale et al. 2004), suggesting that grazing pressure could

have regulated *Pseudo-nitzschia* spp. abundance in the iron addition treatments. It is generally thought that diatoms are too large to be grazed upon by microzooplankton. Yet, significant control of diatom biomass by ciliate and dinoflagellate grazing has been observed in multiple iron addition experiments (Landry et al. 2000b; a; Coale et al. 2004; Saito et al. 2005). Net growth rates of diatoms in the $FeCl_3$ treatment reached 0.94 d^{-1}, suggesting that grazing could not keep up with diatom growth in this treatment. Net growth rates were lower (0.47 d^{-1}) and the biomass of ciliates 20- 29 µm (including tintinnids) higher in the river plume treatment (Figure 16; data obtained from Suzanne Strom). Unless these ciliates preferentially grazed *Pseudo-nitzschia* spp., it is unlikely that top-down regulation drove diatom community composition in the river plume treatment because *Pseudo-nitzschia* spp. and small, chain forming *Rhizosolenia* spp. were of similar size.

A more tenable hypothesis is that reduced *Pseudo-nitzschia* spp. abundance in the river plume treatment directly results from differences in the acquisition, storage, and/or utilization of the $FeCl_3$ and the river plume iron source. Iron acquisition and storage strategies vary across diatom species. It is possible that the Copper River plume iron source favored the acquisition strategies of *Rhizosolenia* spp. over those of *Pseudo-nitzschia* spp. and gave *Rhizosolenia* spp. a competitive advantage in the river plume treatment. Alternatively, detriments to iron acquisition strategies utilized by *Pseudo-nitzschia* spp. could explain its low abundance in the river plume treatment. Marchetti et al. (2009) suggest that the success of *Pseudo-nitzschia* spp. in iron addition experiments may be due to the production of the iron storage protein, ferritin. Ferritin genes are upregulated under iron-replete conditions, allowing *Pseudo-nitzschia* spp. to store more iron than centric diatoms (e.g., *Thalassiosira* spp.). In order for ferritin to store iron, iron must first be removed from bound ligands (likely through reduction mechanisms) and oxidized

to Fe(III) at the cell wall (Pfaffen et al. 2013). If the added $FeCl_3$ was bound by weaker organic ligands, relative to the fluvial source, or incompletely bound to strong ligands, then this iron may have been more accessible to *Pseudo-nitzschia* spp. than the fluvial source. In this way, ferritin production may have given *Pseudo-nitzschia* spp. a competitive advantage over centric diatoms in the $FeCl_3$ treatment, while conferring no advantage in the river plume treatment.

Competitive exclusion of *Pseudo-nitzschia* spp. by bacterio-plankton may have also reduced *Pseudo-nitzschia* spp. abundance in the river plume treatment. Domoic acid production by toxigenic *Pseudo-nitzschia* spp. acts as an organic ligand to give *Pseudo-nitzschia* spp. a competitive advantage in iron-limiting environments (Rue and Bruland 2001). It also plays a key role in chelating Cu for use in the unique high-affinity iron uptake system employed by *Pseudo-nitzschia* spp. This uptake system utilizes a Cu-dependent oxidase to re-oxidize Fe(II) reductively removed from ambient ligands back to Fe(III) immediately prior to intracellular transport and is most successful in conditions with high copper concentrations (Wells et al. 2005). However, in an assemblage of plankton, siderophores produced by bacterio-plankton to bind iron and copper (Wilhelm and Trick 1994; Moffett and Brand 1996) may competitively inhibit iron uptake by *Pseudo-nitzschia* spp. in environments rich in copper. With elevated copper concentrations in the river plume treatment, it is possible that *Pseudo-nitzschia* spp. growth was inhibited by decreased access to strongly complexed iron. Overall, diatom community composition in the river plume treatment was likely dictated primarily by bottom-up regulation stemming from trace metal toxicity and/or iron availability related to synergies between dissolved iron and copper (or other trace metals), taxon-specific iron acquisition strategies, and differences in the lability of iron chemical species (e.g., iron size speciation and ligand binding strength).

Growth and Physiology of Cells < 20 µm

It is hypothesized that cells < 5 µm are adapted to HNLC regions due to their large surface area: volume ratio (Morel et al. 1991). Previous iron addition experiments support this hypothesis and demonstrate minimal response in cells of this size class (de Baar 2005). In our experiment, increased net growth rates and photosynthetic efficiency for cells < 5 µm in response to the $FeCl_3$ and Copper River plume iron sources suggest repair of photosynthetic apparati, including de novo synthesis of proteins in the photosynthetic pathway (Greene et al. 1994), enhanced C fixation, and the overall amelioration of photo-oxidative stress for small cells. Increases in cell size and photosynthetic pigment content for cells < 5 µm in response to iron addition (Table 6) further support the notion that pico- and nanoeukaryotes were iron stressed *in situ*. In contrast to phytoplankton > 20 µm, the $FeCl_3$ and river plume iron sources were able to ameliorate this iron stress to equal extents.

Under iron limitation, iron-containing antioxidants are downregulated, allowing greater ROS damage to the photosynthetic apparatus of phytoplankton (Canini et al. 1992; Martínez 2007). Under iron-replete conditions, it is reasonable to expect decreases in intracellular ROS content in association with increased photosynthetic efficiency. This relationship was observed for pico- and nanoeukaryotes in response to both the $FeCl_3$ and the river plume iron source, but not for *Synechococcus* sp. Both iron sources promoted increased net growth, cell size, and phycoerythrin production in the absence of oxidative stress, suggesting that *Synechococcus* sp. may have been constrained by iron availability but not iron- stressed *in situ*. Because our study failed to differentiate between the photo-physiology of *Synechococcus* sp. and pico- and nanoeukaryotes, it is difficult to ascertain relationships between taxon-specific ROS production and photosynthetic efficiency. Since pico- and nanoeukaryotes outnumbered *Synechococcus* sp.

nearly 10:1, changes in photosynthetic efficiency across treatment primarily reflect the altered physiology of pico- and nanoeukaryotes in response to iron addition. However, the photosynthetic efficiency for cells < 5 µm were similar between the $FeCl_3$ and control treatments at 0 h, suggesting that these cells may not have been particularly iron stressed *in situ*. Further studies to isolate changes in photosynthetic efficiency and specific growth rates for *Synechococcus* sp. in response to iron addition will help confirm whether these cells can experience iron stress in HNLC waters. Even with uncertainty regarding iron- stressed *Synechococcus* sp., the results of our study refute the hypothesis that *all* cells with small surface area: volume ratios are ideally adapted to HNLC regions and highlight differences in the response to iron addition across major ultraplankton groups.

The lack of oxidative stress in *Synechococcus* sp. suggests that *Synechococcus* sp. are well adapted to acquire iron in the HNLC regions of the NGA. Both experimental and modeling approaches have determined that complexation to organic ligands is necessary to maintain iron in solution, and thus increase its residence time in surface seawaters and its availability to biota (Chen et al. 2004; Tagliabue and Arrigo 2006). There is recent evidence that both coastal and HNLC *Synechococcus* sp. produce siderophores that bind dissolved iron and return it to the cell (Berube et al. 2018; Ahlgren et al. 2019). Under iron limited regimes, *Synechococcus* sp. increase production of multiple siderophores with high affinity for iron (Wilhelm and Trick 1994). Diatoms also produce organic ligands (Hopkinson and Morel 2009), but to date, ligand production has not been observed in nanoflagellates. There is evidence suggesting that pico- and nanoeukaryotes can obtain iron from organic ligands via a direct reduction mechanism. However, Hutchins et al. (1999) suggest that the bioavailability of siderophore-bound iron to small eukaryotes is very low. Siderophore production was not directly measured in our study, but

it is possible that these ligands conferred a competitive advantage to *Synechococcus* sp., eliminating any ROS response to iron addition.

Despite the amelioration of iron stress for pico- and nanoeukaryotes, net growth rates for cells < 5 µm remained lower in all treatments, relative to cells > 20 µm, indicating a top-down mechanism regulated these populations. As abundance increased during the first 72 h, pico- and nanoeukaryotes likely exerted a strong grazing pressure on *Synechococcus* sp. The majority of pico- and nanoeukaryotes < 10 µm are mixotrophic, combining photosynthesis with heterotrophy, and can ingest *Synechococcus* sp. (Hana Busse, unpublished data). It is likely that mixotrophs also played a role in regulating *Synechococcus* sp. (see below). Grazer biomass (dinoflagellates < 30 µm and ciliates 20- 39 µm) increased throughout the incubation (Figure 16) and also likely regulated *Synechococcus* sp. Decreased pico- and nanoeukaryote abundance coincided with a bloom of tintinnid ciliates (Figure 16), suggesting that tintinnids may have regulated small eukaryotes in the current study. Trophic cascades involving microzooplankton, pico- and nanoeukaryotes, and their *Synechococcus* sp. prey have been observed in nearly all previous iron addition experiments (see de Baar 2005 and references therein). Microzooplankton grazing also facilitates iron remineralization (Hutchins and Bruland 1994; Barbeau et al. 2001; Dalbec and Twining 2009) and may have provided cells < 5 µm in the control with a source of bioavailable iron, reducing photo-oxidative stress at 72 h. While bottom-up regulation (i.e. iron availability) strongly influenced the physiology of phytoplankton < 5 µm, top-down regulation likely dictated ultraplankton abundance and community composition in our experiment.

Contextualizing the Iron Addition Experiment

Pico- and nanoeukaryotes were more stressed in our experiment than *in* situ. Increased stress in pico- and nanoeukaryote cells in the experiment was likely caused by synergies involving reduced iron availability and deleterious bottle effects (i.e., reduced PAR and decreased mixing).

Fv/Fm decreased in the control during the first 48 h and coincided with increasing pico- and nanoeukaryote chlorophyll *a* content. Fv/Fm also decreased precipitously for cells > 20 µm in the first 48 h. Decreased PAR in screened bottles, relative to *in situ*, and a variable light regime (Figure S2) likely contributed to this photo-physiological response. The average attenuation coefficient for surface waters in the NGA with chlorophyll *a* biomass ~ 0.27 µg L^{-1} (0 h chlorophyll *a* biomass in the control) was 0.17 m^{-1}, corresponding to a 50 % PAR depth of 4.0 m. Intense summer stratification throughout the NGA often inhibits the mixing of surface waters to depths below ~ 15- 20 m. As a result, phytoplankton collected from the surface, and adapted to surface-level PAR, likely received less PAR in screened bottles than they did *in situ*. Daily PAR in the first 48 h of the experiment also varied more per hour than it did in the days leading up to sample collection (Figure S2). These observations suggest that cells < 5 µm and > 20 µm were light-stressed during the beginning of the incubation. Though the plastic response of phytoplankton to low-light regimes might have allowed for photo-acclimation under iron-replete conditions, intracellular iron requirements of phytoplankton increase under low-light conditions (Maldonado et al. 1999). Without a readily available source of iron, pico- and nanoeukaryotes and diatoms in the control likely experienced iron-light colimitation leading to photo-oxidative stress and decreased photosynthetic efficiencies within the first 48 h. After 48 h, photosynthetic efficiency partially recovered, indicating that the HNLC phytoplankton community may have

photo-acclimated to the new light regime with the recycling of dissolved iron or that the variable light regime selected for species tolerant of low light.

In contrast to pico- and nanoeukaryotes, *Synechococcus* sp. were less stressed in the control treatment than *in situ* on LTER transect stations. These results indicate that offshore *Synechococcus* sp. may be better adapted to oligotrophic waters than their coastal counterparts. Further study is needed to better characterize cross-shelf *Synechococcus* sp. communities and their resilience to macronutrient and Fe limitation, but these results corroborate those of the iron addition experiment and suggest that *Synechococcus* sp. may be more adapted to Fe limitation than to N limitation.

Iron Bioavailability in the NGA Ecosystem

Multiple iron addition experiments in all major HNLC regions demonstrate that large diatoms requiring 0.2 – 1.2 nM iron to bloom are highly dependent on iron input from dust deposition (Duce and Tindale 1991a; Jickells and Spokes 2001), oceanic fronts (de Baar 1995), eddy-induced upwelling (Lippiatt et al. 2011), or freshwater input and subsequent cross-shelf exchange (Gerringa et al. 2012). Despite the importance of iron to diatom productivity, iron addition experiments have yet to consider differences in the bioavailability of $FeCl_3$ and freshwater iron sources as a driver of phytoplankton community structure and ecosystem productivity. Despite the ability of the $FeCl_3$ and river plume iron sources to alleviate iron stress for phytoplankton in both the > 20- and < 20 µm size classes, differences in nutrient utilization and productivity efficiencies highlight fundamentally different ecological fates for these two iron sources. Total chlorophyll *a* production efficiencies (Δ Total Chlorophyll *a*: Δ dFe) and N:dFe utilization ratios were highest in the river plume treatment, indicating that the Copper River

plume iron source stimulated more new production than did $FeCl_3$. While new production in the $FeCl_3$ treatment was shunted directly into diatom biomass, new production in the river plume treatment, where chlorophyll *a* > 20 µm comprised only 29 % of total biomass (Figure 3E), was predominantly retained in the < 5 µm size class. Trends in Si:N utilization ratios also reflect changes in total community composition dictated by iron source. Average Si:N utilization ratios in both the river plume and $FeCl_3$ treatment were above the expected 1:1 Redfield-Brzezinski ratio (Brzezinski 2004), indicating decoupling of Si and N use. This decoupling could result from changes in diatom physiology, larger N drawdown by small phytoplankton than by diatoms, and/or a heavy silification of diatoms (Franck et al. 2005). Decoupling of Si and N use in the $FeCl_3$ treatment was likely driven by thickening of diatom frustules in response to environmental stress (e.g. macronutrient depletion) and/or by a diatom community dominated by heavily silicified cells (Franck et al. 2005). In contrast, Si:N utilization ratios in the river plume treatment were likely dictated by increased N utilization by small phytoplankton, relative to diatoms. These results demonstrate that $FeCl_3$ and fluvial iron input result in divergent phytoplankton community structures with implications for phytoplankton ecology in the NGA HNLC region.

Huge annual suspended sediment loads (~ 4 % of which is iron, by weight) are sourced to the NGA from the surrounding glaciers through freshwater inputs (Milliman and Syvitski 1992; Wu et al. 2009). Stabeno et al. (2004) hypothesize that offshore transport of fluvial iron is the major driver of iron input to the NGA HNLC region in summer and Lam et al. (2006) indicate that the North Pacific is primed for lateral transport of coastal waters into the open subarctic due to a permanent pycnocline at ~ 150 m. Though diatom blooms have been documented in North Pacific HNLC regions and have been linked to natural iron fertilization by iron from the continental shelf (Johnson et al. 1999; Lam et al. 2006), it seems unlikely that iron from the

Copper River plume is capable of producing similar diatom blooms in the HNLC waters of the NGA. While diatoms were less stressed when exposed to the river plume iron source, indicating an increased capacity for growth (Krause and Weis 1984), the fluvial iron source favored the production of small cell biomass, at least over the 5 d period of our incubation experiment. Results of this experiment suggest that diatom physiology and growth measured in previous iron addition experiments in response to $FeCl_3$ do not directly translate to natural iron sources, in particular glacier river sources. Diatom productivity has significant implications for food web structure and secondary productivity in the NGA (Strom et al. 2016). To understand the variability in primary and secondary productivity in the NGA, it is imperative that iron limitation of diatoms be modeled not only as a function of spatio-temporal variability in dissolved iron concentrations, but also differential source-dependent bioavailability across both cell size (as in Fiechter et al. 2009) and taxa.

High turnover of phytoplankton < 5 µm production via grazing has significant implications for NGA food web dynamics. Grazing of *Synechococcus* sp. was likely dominated by nanoflagellates. Mixotrophy has been documented in nearly all nanoflagellates (2- 10 µm) in the NGA (Hana Busse, unpublished data). Nanoflagellates are known to readily ingest *Synechococcus* sp. and bacterial (including cyanobacterial) ingestion has been hypothesized as an iron-acquisition strategy for some of these small eukaryotes (Maranger et al. 1998). Because of their ability to reduce nutrient export and increase nutrient turnover in surface waters, mixotrophic nanoflagellates can increase productivity in oligotrophic regions (Hartmann et al. 2012). Pico- and nanoeukaryotes were grazed upon, likely by dinoflagellates < 30 µm and a variety of ciliates. The role of large micrograzers in the transfer of primary production has been well documented in the NGA and in open oceans (Calbet and Landry 2004; Strom et al. 2007;

Calbet 2008). Through its benefits on ultraplankton productivity and subsequent predator-prey dynamics, episodic input from the Copper River may contribute to the persistent presence of ultraplankton and help stabilize the community in HNLC waters. Fluvial iron input may also prime the rapid transport of biomass into secondary production through micrograzer intermediates upon the introduction of highly bioavailable iron. In this way, iron from the Copper River plume represents an important contributor to the characteristic variability of primary production in the NGA despite its relatively low bioavailability to diatoms.

LITERATURE CITED

Achterberg, E. P., C. M. Moore, S. A. Henson, and others. 2013. Natural iron fertilization by the Eyjafjallajökull volcanic eruption. Geophysical Research Letters **40**: 921–926.

Aguilar-Islas, A. M., M. J. M. Séguret, R. Rember, K. N. Buck, P. Proctor, C. W. Mordy, and N. B. Kachel. 2016. Temporal variability of reactive iron over the Gulf of Alaska shelf. Deep Sea Research Part II: Topical Studies in Oceanography **132**: 90–106. doi:10.1016/j.dsr2.2015.05.004

Aguilar-Islas, A. M., J. Wu, R. Rember, A. M. Johansen, and L. M. Shank. 2010. Dissolution of aerosol-derived iron in seawater: Leach solution chemistry, aerosol type, and colloidal iron fraction. Marine Chemistry **120**: 25–33. doi:10.1016/j.marchem.2009.01.011

Ahlgren, N. A., B. S. Belisle, and M. D. Lee. 2019. Genomic mosaicism underlies the adaptation of marine Synechococcus ecotypes to distinct oceanic iron niches. Environmental Microbiology **n/a**. doi:10.1111/1462-2920.14893

Allen, A. E., J. LaRoche, U. Maheswari, and others. 2008. Whole-cell response of the pennate diatom Phaeodactylum tricornutum to iron starvation. Proceedings of the National Academy of Sciences **105**: 10438–10443. doi:10.1073/pnas.0711370105

Anderson, P. J., and J. F. Piatt. 1999. Community reorganization in the Gulf of Alaska following ocean climate regime shift. Marine Ecology Progress Series **189**: 117–123.

Apel, K., and H. Hirt. 2004. Reactive Oxygen Species: Metabolism, Oxidative Stress, and Signal Transduction. Annual Review of Plant Biology **55**: 373–399. doi:10.1146/annurev.arplant.55.031903.141701

Argüelles, M., C. Benavides, and I. Fernández. 2014. A new approach to the identification of regional clusters: hierarchical clustering on principal components. Applied Economics **46**: 2511–2519. doi:10.1080/00036846.2014.904491

Armstrong, F. A. J., C. R. Stearns, and J. D. H. Strickland. 1967. The measurement of upwelling and subsequent biological process by means of the Technicon Autoanalyzer® and associated equipment. *Deep Sea Research and Oceanographic Abstracts*. Elsevier. 381–389.

Assmy, P. 2004. Temporal development and vertical distribution of major components of the plankton assemblage during an iron fertilization experiment in the Antarctic Polar Frontal Zone. PhD Thesis. Universität Bremen.

de Baar, H. J., A. G. Buma, R. F. Nolting, G. C. Cadée, G. Jacques, and P. J. Tréguer. 1990. On iron limitation of the Southern Ocean: experimental observations in the Weddell and Scotia Seas. Marine ecology progress series 105–122.

de Baar, H. J. W. 1995. Importance of iron for phytoplankton spring blooms and CO2 drawdown in the Southern Ocean. Nature **373**: 412–415.

de Baar, H. J. W. 2005. Synthesis of iron fertilization experiments: From the Iron Age in the Age of Enlightenment. J. Geophys. Res. **110**: C09S16. doi:10.1029/2004JC002601

Banse, K. 1990. Does iron really limit phytoplankton production in the offshore subarctic Pacific? Limnology and Oceanography **35**: 772–775.

Barbeau, K., E. L. Rue, K. W. Bruland, and A. Butler. 2001. Photochemical cycling of iron in the surface ocean mediated by microbial iron(III)-binding ligands. Nature **413**: 409–413. doi:10.1038/35096545

Behrenfeld, M. J., A. J. Bale, Z. S. Kolber, J. Aiken, and P. G. Falkowski. 1996. Confirmation of iron limitation of phytoplankton photosynthesis in the equatorial Pacific Ocean. Nature **383**: 508–511.

Ben-Hur, A., and I. Guyon. 2003. Detecting Stable Clusters Using Principal Component Analysis, p. 159–182. *In* Functional Genomics. Humana Press.

Berube, P. M., S. J. Biller, T. Hackl, and others. 2018. Single cell genomes of Prochlorococcus , Synechococcus , and sympatric microbes from diverse marine environments. Scientific Data **5**: 1–11. doi:10.1038/sdata.2018.154

Bholowalia, P., and A. Kumar. 2014. EBK-means: A clustering technique based on elbow method and k-means in WSN. International Journal of Computer Applications **105**.

Booth, B. C. 1988. Size classes and major taxonomic groups of phytoplankton at two locations in the subarctic Pacific Ocean in May and August, 1984. Marine Biology **97**: 275–286.

Boyd, P. W., T. Jickells, C. S. Law, and others. 2007. Mesoscale Iron Enrichment Experiments 1993-2005: Synthesis and Future Directions. Science **315**: 612–617. doi:10.1126/science.1131669

Boyd, P. W., C. S. Law, C. S. Wong, and others. 2004. The decline and fate of an iron-induced subarctic phytoplankton bloom. Nature **428**: 549.

Boyd, P. W., D. L. Muggli, D. E. Varela, R. H. Goldblatt, R. Chretien, K. J. Orians, and P. J. Harrison. 1996. In vitro iron enrichment experiments in the NE subarctic Pacific. Marine Ecology Progress Series **136**: 179–193.

Brand, L. Reduction of marine phytoplankton reproduction rates by copper and cadmium. 27.

Brickley, P. J., and A. C. Thomas. 2004. Satellite-measured seasonal and inter-annual chlorophyll variability in the Northeast Pacific and Coastal Gulf of Alaska. Deep Sea Research Part II: Topical Studies in Oceanography **51**: 229–245.

Brzezinski, M. A. 2004. The Si:C:N ratio of marine diatoms: Interspecific variability and the effect of some environmental variables. Journal of Phycology **21**: 347–357. doi:10.1111/j.0022-3646.1985.00347.x

Calbet, A. 2008. The trophic roles of microzooplankton in marine systems. ICES J. Mar. Sci. **65**: 325–331. doi:10.1093/icesjms/fsn013

Calbet, A., and M. R. Landry. 2004. Phytoplankton growth, microzooplankton grazing, and carbon cycling in marine systems. Limnology and Oceanography **49**: 51–57. doi:10.4319/lo.2004.49.1.0051

Canini, A., P. Civitareale, S. Marini, M. G. Caiola, and G. Rotilio. 1992. Purification of iron superoxide dismutase from the cyanobacterium Anabaena cylindrica Lemm. and localization of the enzyme in heterocysts by immunogold labeling. Planta **187**: 438–444.

Cavender-Bares, K. K., E. L. Mann, S. W. Chisholm, M. E. Ondrusek, and R. R. Bidigare. 1999. Differential response of equatorial Pacific phytoplankton to iron fertilization. Limnology and Oceanography **44**: 237–246.

Chavez, F. P. 1989. Size distribution of phytoplankton in the central and eastern tropical Pacific. Global Biogeochemical Cycles **3**: 27–35.

Cheloni, G., C. Cosio, and V. I. Slaveykova. 2014. Antagonistic and synergistic effects of light irradiation on the effects of copper on Chlamydomonas reinhardtii. Aquatic Toxicology **155**: 275–282. doi:10.1016/j.aquatox.2014.07.010

Chen, M., W.-X. Wang, and L. Guo. 2004. Phase partitioning and solubility of iron in natural seawater controlled by dissolved organic matter. Global biogeochemical cycles **18**.

Coale, K. H. 1991. Effects of iron, manganese, copper, and zinc enrichments on productivity and biomass in the subarctic Pacific. Limnology and Oceanography **36**: 1851–1864. doi:10.4319/lo.1991.36.8.1851

Coale, K. H., K. S. Johnson, F. P. Chavez, and others. 2004. Southern Ocean iron enrichment experiment: carbon cycling in high-and low-Si waters. science **304**: 408–414.

Collier, J. L., and B. Palenik. 2003. Phycoerythrin-containing picoplankton in the Southern California Bight. Deep Sea Research Part II: Topical Studies in Oceanography **50**: 2405–2422.

Crusius, J., A. W. Schroth, S. Gassó, C. M. Moy, R. C. Levy, and M. Gatica. 2011. Glacial flour dust storms in the Gulf of Alaska: Hydrologic and meteorological controls and their importance as a source of bioavailable iron. Geophysical Research Letters **38**: n/a-n/a. doi:10.1029/2010GL046573

Dalbec, A., and B. Twining. 2009. Remineralization of bioavailable iron by a heterotrophic dinoflagellate. Aquat. Microb. Ecol. **54**: 279–290. doi:10.3354/ame01270

Donaghay, P. L., P. S. Liss, R. A. Duce, D. R. Kester, A. K. Hanson, T. Villareal, N. W. Tindale, and D. J. Gifford. 1991. The role of episodic atmospheric nutrient inputs in the chemical and biological dynamics of oceanic ecosystems. Oceanography **4**: 62–70.

Doucette, G. J., and P. J. Harrison. 1990. Some effects of iron and nitrogen stress on the red tide dinoflagellate Gymnodinium sanguineum. Marine ecology progress series. Oldendorf **62**: 293–306.

Dubelaar, G. B., and R. R. Jonker. 2000. Flow cytometry as a tool for the study of phytoplankton. Scientia Marina **64**: 135–156.

Duce, R. A. 1986. The impact of atmospheric nitrogen, phosphorus, and iron species on marine biological productivity, p. 497–529. *In* The role of air-sea exchange in geochemical cycling. Springer.

Duce, R. A., and N. W. Tindale. 1991a. Atmospheric transport of iron and its deposition in the ocean. Limnology and oceanography **36**: 1715–1726.

Duce, R. A., and N. W. Tindale. 1991b. Chemistry and biology of iron and other trace metals. Limnol. Oceanogr **36**: 1715–1726.

Eppley, R. W. 1972. Temperature and phytoplankton growth in the sea. Fish. bull **70**: 1063–1085.

Erdner, D. L., and D. M. Anderson. 1999. Ferredoxin and flavodoxin as biochemical indicators of iron limitation during open-ocean iron enrichment. Limnology and Oceanography **44**: 1609–1615. doi:10.4319/lo.1999.44.7.1609

Fiechter, J., A. M. Moore, C. A. Edwards, and others. 2009. Modeling iron limitation of primary production in the coastal Gulf of Alaska. Deep Sea Research Part II: Topical Studies in Oceanography **56**: 2503–2519. doi:10.1016/j.dsr2.2009.02.010

Franck, V. M., G. J. Smith, K. W. Bruland, and M. A. Brzezinski. 2005. Comparison of size-dependent carbon, nitrate, and silicic acid uptake rates in high-and low-iron waters. Limnology and Oceanography **50**: 825–838.

Geider, R. J., and J. La Roche. 1994. The role of iron in phytoplankton photosynthesis, and the potential for iron-limitation of primary productivity in the sea. Photosynthesis research **39**: 275–301.

Gerringa, L. J., A.-C. Alderkamp, P. Laan, and others. 2012. Iron from melting glaciers fuels the phytoplankton blooms in Amundsen Sea (Southern Ocean): Iron biogeochemistry. Deep Sea Research Part II: Topical Studies in Oceanography **71**: 16–31.

Glover, H. 1977. Effects of iron deficiency on Isochrysis galbana (Chrysophyceae) and Phaeodactylum tricornutum (Bacillariophyceae)[Algae]. Journal of Phycology.

Greene, R. M., R. J. Geider, and P. G. Falkowski. 1991. Effect of iron limitation on photosynthesis in a marine diatom. Limnology and Oceanography **36**: 1772–1782.

Greene, R. M., R. J. Geider, Z. Kolber, and P. G. Falkowski. 1992. Iron-induced changes in light harvesting and photochemical energy conversion processes in eukaryotic marine algae. Plant Physiology **100**: 565–575.

Greene, R. M., Z. S. Kolber, D. G. Swift, N. W. Tindale, and P. G. Falkowski. 1994. Physiological limitation of phytoplankton photosynthesis in the eastern equatorial Pacific determined from variability in the quantum yield of fluorescence. Limnology and Oceanography **39**: 1061–1074.

Guikema, J. A., and L. A. Sherman. 1983. Organization and function of chlorophyll in membranes of cyanobacteria during iron starvation. Plant Physiology **73**: 250–256.

Hartmann, M., C. Grob, G. A. Tarran, A. P. Martin, P. H. Burkill, D. J. Scanlan, and M. V. Zubkov. 2012. Mixotrophic basis of Atlantic oligotrophic ecosystems. PNAS **109**: 5756–5760. doi:10.1073/pnas.1118179109

Hecky, R. E., and P. Kilham. 1988. Nutrient limitation of phytoplankton in freshwater and marine environments: A review of recent evidence on the effects of enrichment. Limnology and Oceanography **33**: 796–822. doi:10.4319/lo.1988.33.4part2.0796

Helbling, E. W., V. Villafañe, and O. Holm-Hansen. 1991. Effect of iron on productivity and size distribution of Antarctic phytoplankton. Limnology and Oceanography **36**: 1879–1885. doi:10.4319/lo.1991.36.8.1879

Henson, S. A. 2007. Water column stability and spring bloom dynamics in the Gulf of Alaska. Journal of Marine Research **65**: 715–736.

Hopkinson, B. M., and F. M. M. Morel. 2009. The role of siderophores in iron acquisition by photosynthetic marine microorganisms. Biometals **22**: 659–669. doi:10.1007/s10534-009-9235-2

Hudson, R. J., and F. M. Morel. 1990. lron transport in marine phytoplankton: Kinetics of cellular and medium coordination reactions. Limnology and Oceanography **35**: 1002–1020.

Hutchins, D. A., and K. W. Bruland. 1998. Iron-limited diatom growth and Si: N uptake ratios in a coastal upwelling regime. Nature **393**: 561.

Hutchins, D. A., V. M. Franck, M. A. Brzezinski, and K. W. Bruland. 1999. Inducing phytoplankton iron limitation in iron-replete coastal waters with a strong chelating ligand. Limnol. Oceanogr. **44**: 1009–1018. doi:10.4319/lo.1999.44.4.1009

Hutchins, D., and K. Bruland. 1994. Grazer-mediated regeneration and assimilation of Fe, Zn and Mn from planktonic prey. Mar. Ecol. Prog. Ser. **110**: 259–269. doi:10.3354/meps110259

Ivanochko, T. 2012. Phyto'pedia- The Phytoplankton Encyclopedia Project.

Janout, M. A., T. J. Weingartner, T. C. Royer, and S. L. Danielson. 2010. On the nature of winter cooling and the recent temperature shift on the northern Gulf of Alaska shelf. Journal of Geophysical Research: Oceans **115**. doi:10.1029/2009JC005774

Jickells, T. D., and L. J. Spokes. 2001. Atmospheric iron inputs to the oceans, p. 85–121. *In* D.R. Turner and K. Hunter [eds.], The Biogeochemistry of Iron in Seawater. Wiley.

Johnson, K. S., F. P. Chavez, and G. E. Friederich. 1999. Continental-shelf sediment as a primary source of iron for coastal phytoplankton. Nature **398**: 697–700. doi:10.1038/19511

Kaczmarska, I. 2001. Guide D'Identification du Phytoplancton Marin de l'Estuaire et du Golfe du Saint-Laurent, Incuant Egalement Certains Protozoaires. Journal of Phycology **37**: 922–923. doi:10.1046/j.1529-8817.2001.03751.x

Kazamia, E., R. Sutak, J. Paz-Yepes, and others. 2018. Endocytosis-mediated siderophore uptake as a strategy for Fe acquisition in diatoms. Science advances **4**: eaar4536.

Krause, G. H., and E. Weis. 1984. Chlorophyll fluorescence as a tool in plant physiology. Photosynthesis research **5**: 139–157.

Ladd, C., P. Stabeno, and E. D. Cokelet. 2005. A note on cross-shelf exchange in the northern Gulf of Alaska. Deep Sea Research Part II: Topical Studies in Oceanography **52**: 667–679. doi:10.1016/j.dsr2.2004.12.022

Lagerloef, G. S. 1995. Interdecadal variations in the Alaska Gyre. Journal of Physical Oceanography **25**: 2242–2258.

Lam, P. J., J. K. B. Bishop, C. C. Henning, M. A. Marcus, G. A. Waychunas, and I. Y. Fung. 2006. Wintertime phytoplankton bloom in the subarctic Pacific supported by continental margin iron. Global Biogeochemical Cycles **20**: n/a-n/a. doi:10.1029/2005GB002557

Landry, M., M. Ondrusek, S. Tanner, S. Brown, J. Constantinou, R. Bidigare, K. Coale, and S. Fitzwater. 2000a. Biological response to iron fertilization in the eastern equatorial Pacific (IronEx II). I.

Microplankton community abundances and biomass. Mar. Ecol. Prog. Ser. **201**: 27–42. doi:10.3354/meps201027

Landry, M. R., J. Constantinou, M. Latasa, S. L. Brown, R. R. Bidigare, and M. E. Ondrusek. 2000b. Biological response to iron fertilization in the eastern equatorial Pacific (IronEx II). III. Dynamics of phytoplankton growth and microzooplankton grazing. Marine Ecology Progress Series **201**: 57–72.

Lelong, A., E. Bucciarelli, H. Hégaret, and P. Soudant. 2013. Iron and copper limitations differently affect growth rates and photosynthetic and physiological parameters of the marine diatom *Pseudo-nitzschia delicatissima*. Limnol. Oceanogr. **58**: 613–623. doi:10.4319/lo.2013.58.2.0613

Lelong, A., D. F. Jolley, P. Soudant, and H. Hégaret. 2012. Impact of copper exposure on Pseudo-nitzschia spp. physiology and domoic acid production. Aquatic Toxicology **118–119**: 37–47. doi:10.1016/j.aquatox.2012.03.010

Lesser, M. P. 2006. Oxidative stress in marine environments: Biochemistry and Physiological Ecology. Annual Review of Physiology **68**: 253–278. doi:10.1146/annurev.physiol.68.040104.110001

Lippiatt, S. M., M. T. Brown, M. C. Lohan, and K. W. Bruland. 2011. Reactive iron delivery to the Gulf of Alaska via a Kenai eddy. Deep Sea Research Part I: Oceanographic Research Papers **58**: 1091–1102.

Lippiatt, S. M., M. C. Lohan, and K. W. Bruland. 2010. The distribution of reactive iron in northern Gulf of Alaska coastal waters. Marine Chemistry **121**: 187–199. doi:10.1016/j.marchem.2010.04.007

Liu, H., M. J. Dagg, and S. Strom. 2005. Grazing by the calanoid copepod Neocalanus cristatus on the microbial food web in the coastal Gulf of Alaska. Journal of Plankton Research **27**: 647–662. doi:10.1093/plankt/fbi039

Liu, W., D. W. Au, D. M. Anderson, P. K. Lam, and R. S. Wu. 2007. Effects of nutrients, salinity, pH and light: dark cycle on the production of reactive oxygen species in the alga Chattonella marina. Journal of experimental marine biology and ecology **346**: 76–86.

Lundholm, N., and G. R. Hasle. 2010. Fragilariopsis (Bacillariophyceae) of the Northern Hemisphere – morphology, taxonomy, phylogeny and distribution, with a description of F. pacifica sp. nov. Phycologia **49**: 438–460. doi:10.2216/09-97.1

Lundholm, N., J. Skov, R. Pocklington, and Ø. Moestrup. 1997. Studies on the marine planktonic diatom Pseudo-nitzschia. 2. Autecology of P. pseudodelicatissima based on isolates from Danish coastal waters. Phycologia **36**: 381–388. doi:10.2216/i0031-8884-36-5-381.1

Mackey, K. R. M., K. N. Buck, J. R. Casey, A. Cid, M. W. Lomas, Y. Sohrin, and A. Paytan. 2012. Phytoplankton responses to atmospheric metal deposition in the coastal and open-ocean Sargasso Sea. Front. Microbiol. **3**. doi:10.3389/fmicb.2012.00359

Maldonado, M. T., P. W. Boyd, P. J. Harrison, and N. M. Price. 1999. Co-limitation of phytoplankton growth by light and Fe during winter in the NE subarctic Pacific Ocean. Deep Sea Research Part II: Topical Studies in Oceanography **46**: 2475–2485. doi:10.1016/S0967-0645(99)00072-7

Mallick, N., and F. H. Mohn. 2000. Reactive oxygen species: response of algal cells. Journal of Plant Physiology **157**: 183–193. doi:10.1016/S0176-1617(00)80189-3

Maranger, R., D. F. Bird, and N. M. Price. 1998. Iron acquisition by photosynthetic marine phytoplankton from ingested bacteria. Nature **396**: 248–251. doi:10.1038/24352

Marchetti, A., M. S. Parker, L. P. Moccia, and others. 2009. Ferritin is used for iron storage in bloom-forming marine pennate diatoms. Nature **457**: 467.

Martin, J. H., and S. E. Fitzwater. 1988. Iron deficiency limits phytoplankton growth in the north-east Pacific subarctic. Nature **331**: 341.

Martin, J. H., R. M. Gordon, S. Fitzwater, and W. W. Broenkow. 1989. Vertex: phytoplankton/iron studies in the Gulf of Alaska. Deep Sea Research Part A. Oceanographic Research Papers **36**: 649–680. doi:10.1016/0198-0149(89)90144-1

Martínez, R. 2007. Effects of ultraviolet radiation on protein content, respiratory electron transport system (ETS) activity and superoxide dismutase (SOD) activity of Antarctic plankton. Polar Biol **30**: 1159–1172. doi:10.1007/s00300-007-0273-3

McKay, R. M. L., J. La Roche, A. F. Yakunin, D. G. Durnford, and R. J. Geider. 1999. Accumulation of ferredoxin and flavodoxin in a marine diatom in repsonse to Fe. Journal of Phycology **35**: 510–519. doi:10.1046/j.1529-8817.1999.3530510.x

Menden-Deuer, S., and E. J. Lessard. 2000. Carbon to volume relationships for dinoflagellates, diatoms, and other protist plankton. Limnol. Oceanogr. **45**: 569–579. doi:10.4319/lo.2000.45.3.0569

Milliman, J. D., and J. P. Syvitski. 1992. Geomorphic/tectonic control of sediment discharge to the ocean: the importance of small mountainous rivers. The journal of Geology **100**: 525–544.

Moffett, J. W., and L. E. Brand. 1996. Production of strong, extracellular Cu chelators by marine cyanobacteria in response to Cu stress. Limnology and Oceanography **41**: 388–395.

Moore, R. M., J. E. Milley, and A. Chatt. 1984. The potential for biological mobilization of trace-elements from aeolian dust in the ocean and its importance in the case of iron. Oceanologica Acta **7**: 221–228.

Morel, F., J. Rueter, and N. Price. 1991. Iron nutrition of phytoplankton and Its possible importance in the ecology of ocean regions with high nutrient and low biomass. Oceanography **4**: 56–61. doi:10.5670/oceanog.1991.03

Murphy, J., and J. P. Riley. 1962. A modified single solution method for the determination of phosphate in natural waters. Analytica chimica acta **27**: 31–36.

Okkonen, S. R., T. J. Weingartner, S. L. Danielson, D. L. Musgrave, and G. M. Schmidt. 2003. Satellite and hydrographic observations of eddy-induced shelf-slope exchange in the northwestern Gulf of Alaska. Journal of Geophysical Research: Oceans **108**: n/a-n/a. doi:10.1029/2002JC001342

Olson, R. J., H. M. Sosik, A. M. Chekalyuk, and A. Shalapyonok. 2000. Effects of iron enrichment on phytoplankton in the Southern Ocean during late summer: active fluorescence and flow cytometric analyses. Deep Sea Research Part II: Topical Studies in Oceanography **47**: 3181–3200.

Pfaffen, S., R. Abdulqadir, N. E. Le Brun, and M. E. Murphy. 2013. Mechanism of ferrous iron binding and oxidation by ferritin from a pennate diatom. Journal of Biological Chemistry **288**: 14917–14925.

Poulin, M., G. Massé, S. T. Belt, P. Delavault, F. Rousseau, J.-M. Robert, and S. J. Rowland. 2004. Morphological, biochemical and molecular evidence for the transfer of Gyrosigma nipkowii Meister to the genus Haslea (Bacillariophyta). European Journal of Phycology **39**: 181–195. doi:10.1080/0967026042000202136

Price, N. M., L. F. Andersen, and F. M. M. Morel. 1991. Iron and nitrogen nutrition of equatorial Pacific plankton. Deep Sea Research Part A. Oceanographic Research Papers **38**: 1361–1378. doi:10.1016/0198-0149(91)90011-4

Reid, R. T., and A. Butler. 1991. Investigation of the mechanism of iron acquisition by the marine bacterium Alteromonas luteoviolaceus: Characterization of siderophore production. Limnology and oceanography **36**: 1783–1792.

Rue, E., and K. Bruland. 2001. Domoic acid binds iron and copper: a possible role for the toxin produced by the marine diatom Pseudo-nitzschia. Marine Chemistry **76**: 127–134.

Rueter, J., and D. R. Ades. 1987. The role of iron nutrition in photosynthesis and nitrogen assimilation in Scenedesmus quadricauda (Chlorophyceae). Journal of Phycology **23**: 452–457.

Saito, H., K. Suzuki, A. Hinuma, T. Ota, K. Fukami, H. Kiyosawa, T. Saino, and A. Tsuda. 2005. Responses of microzooplankton to in situ iron fertilization in the western subarctic Pacific (SEEDS). Progress in Oceanography **64**: 223–236. doi:10.1016/j.pocean.2005.02.010

Salin, M. L. 1988. Toxic oxygen species and protective systems of the chloroplast. Physiologia Plantarum **72**: 681–689.

Shultz, M., J. Piatt, A. Harding, A. Kettle, and T. Van Pelt. 2009. Timing of breeding and reproductive performance in murres and kittiwakes reflect mismatched seasonal prey dynamics. Marine Ecology Progress Series **393**: 247–258. doi:10.3354/meps08136

Stabeno, P. J., N. A. Bond, A. J. Hermann, N. B. Kachel, C. W. Mordy, and J. E. Overland. 2004. Meteorology and oceanography of the Northern Gulf of Alaska. Continental Shelf Research **24**: 859–897. doi:10.1016/j.csr.2004.02.007

Strom, S. L., K. A. Fredrickson, and K. J. Bright. 2016. Spring phytoplankton in the eastern coastal Gulf of Alaska: Photosynthesis and production during high and low bloom years. Deep Sea Research Part II: Topical Studies in Oceanography **132**: 107–121.

Strom, S. L., E. L. Macri, and M. B. Olson. 2007. Microzooplankton grazing in the coastal Gulf of Alaska: Variations in top-down control of phytoplankton. Limnology and Oceanography **52**: 1480.

Strom, S. L., M. B. Olson, E. L. Macri, and C. W. Mordy. 2006. Cross-shelf gradients in phytoplankton community structure, nutrient utilization, and growth rate in the coastal Gulf of Alaska. Marine Ecology Progress Series **328**: 75–92.

Sumaila, U. R., W. W. Cheung, V. W. Lam, D. Pauly, and S. Herrick. 2011. Climate change impacts on the biophysics and economics of world fisheries. Nature climate change **1**: 449.

Sunda, W. 1975. The relationship between cupric ion activity and the toxicity of copper to phytoplankton, Massachusetts Institute of Technology and Woods Hole Oceanographic Institution.

Sunda, W. G., and S. A. Huntsman. 2011. Interactive effects of light and temperature on iron limitation in a marine diatom: Implications for marine productivity and carbon cycling. Limnology and Oceanography **56**: 1475–1488. doi:10.4319/lo.2011.56.4.1475

Suzuki, K., H. Saito, T. Isada, and others. 2009. Community structure and photosynthetic physiology of phytoplankton in the northwest subarctic Pacific during an in situ iron fertilization experiment (SEEDS-II). Deep Sea Research Part II: Topical Studies in Oceanography **56**: 2733–2744.

Tagliabue, A., and K. R. Arrigo. 2006. Processes governing the supply of iron to phytoplankton in stratified seas. Journal of Geophysical Research: Oceans **111**.

Thessen, A. E., Q. Dortch, M. L. Parsons, and W. Morrison. 2005. Effect of salinity on Pseudo-nitzschia species (Bacillariophyceae) growth and distribution. Journal of Phycology **41**: 21–29. doi:10.1111/j.1529-8817.2005.04077.x

Trainer, V. L., S. S. Bates, N. Lundholm, A. E. Thessen, W. P. Cochlan, N. G. Adams, and C. G. Trick. 2012. Pseudo-nitzschia physiological ecology, phylogeny, toxicity, monitoring and impacts on ecosystem health. Harmful Algae **14**: 271–300. doi:10.1016/j.hal.2011.10.025

Vaulot, D., C. Courties, and F. Partensky. 1989. A simple method to preserve oceanic phytoplankton for flow cytometric analyses. Cytometry **10**: 629–635. doi:10.1002/cyto.990100519

Waite, J. N., and F. J. Mueter. 2013. Spatial and temporal variability of chlorophyll-a concentrations in the coastal Gulf of Alaska, 1998–2011, using cloud-free reconstructions of SeaWiFS and MODIS-Aqua data. Progress in Oceanography **116**: 179–192.

Wells, M. L., C. G. Trick, W. P. Cochlan, M. P. Hughes, and V. L. Trainer. 2005. Domoic acid: The synergy of iron, copper, and the toxicity of diatoms. Limnol. Oceanogr. **50**: 1908–1917. doi:10.4319/lo.2005.50.6.1908

Whitney, F. A., W. R. Crawford, and P. J. Harrison. 2005. Physical processes that enhance nutrient transport and primary productivity in the coastal and open ocean of the subarctic NE Pacific. Deep Sea Research Part II: Topical Studies in Oceanography **52**: 681–706.

Wilhelm, S. W., and C. G. Trick. 1994. Iron-limited growth of cyanobacteria: Multiple siderophore production is a common response. Limnology and Oceanography **39**: 1979–1984. doi:10.4319/lo.1994.39.8.1979

Wu, J., A. Aguilar-Islas, R. Rember, T. Weingartner, S. Danielson, and T. Whitledge. 2009. Size-fractionated iron distribution on the northern Gulf of Alaska. Geophysical Research Letters **36**. doi:10.1029/2009GL038304

Young, R. W., K. L. Carder, P. R. Betzer, and others. 1991. Atmospheric iron inputs and primary productivity: Phytoplankton responses in the North Pacific. Global Biogeochemical Cycles **5**: 119–134.

Yuan, C., and H. Yang. 2019. Research on K-Value Selection Method of K-Means Clustering Algorithm. J — Multidisciplinary Scientific Journal **2**: 226–235. doi:10.3390/j2020016

Table 1. Summary of flow cytometric parameters measured for *Synechococcus* sp. and pico- and nanoeukaryotes.

Parameter	Measurement	Normalized?	Biological Interpretation
FSC (Forward Scatter)	Detected by FSC diode in- line with the flow of cells after light passes through a 488 nm bandpass filter	No	Proxy for cell size; typically, larger cells have larger FSC, though FSC may not scale linearly with cell size
FL1 (Green Fluorescence)	Detected by a photomultiplier at λ= 530 nm	Yes, to median bead FL1 and again to mean "Community Composition" FL1	Detected the fluorescence of CellROX™ Green ROS probe. Higher FL1 indicated more ROS content per cell.
FL2 (Yellow-Orange Fluorescence)	Detected by a photomultiplier at λ= 585 nm	Yes, to median bead FL2	Proxy for *Synechococcus* sp. phycoerythrin content
FL3 (Red Fluorescence)	Detected by a photomultiplier at λ= 670 nm	Yes, to median bead FL3	Proxy for *Synechococcus* sp. and nano- and picoeukaryote chlorophyll *a* content

Table 2. Size- fractionated phytoplankton net growth rates. Chlorophyll concentrations from hours 48- 96 were ln-transformed before net growth rates were estimated from ordinary least squares regression coefficients. Exponents indicate treatment groupings at $\alpha = 0.10$ based on Tukey HSD pairwise contrasts. In cases where growth rates differ across treatments (C: Control, I: Iron Chloride, R: River Plume), t-values (df) and p-values are provided.

Size Fraction	Treatment	Net Growth Rate (d^{-1})	p- value
Total	Control	0.31^{A}	$t_{C,I\,(12)} = -5.86$, $p = 0.0002$ $t_{R,I\,(12)} = 3.87$; $p = 0.0058$
	$FeCl_3$	0.78^{B}	
	River	0.47^{A}	
> 20 um	Control	0.36^{A}	$t_{C,I\,(12)} = -3.59$, $p = 0.0095$ $t_{R,I\,(12)} = 2.94$, $p = 0.031$
	$FeCl_3$	0.94^{B}	
	River	0.47^{A}	
5-20 um	Control	0.53^{A}	N.S.
	$FeCl_3$	0.71^{A}	
	River	0.66^{A}	
< 5 µm	Control	0.15^{A}	$t_{C,I\,(12)} = -2.533$, $p = 0.063$
	$FeCl_3$	0.55^{B}	
	River	0.39^{AB}	

Table 3. Size-fractionated photosynthetic efficiency (Fv/Fm). Exponents indicate treatment groupings at $\alpha = 0.10$. With the exception of the control from 0- 48 h, Fv/Fm did not change in any size fraction. In cases where average Fv/Fm differed across treatments (C: Control, I: Iron chloride; R: River plume), p-values are provided.

Size Fraction	Treatment	Average Fv/Fm	p-value
Total	Control	0.40^{A}	$t_{C,I\ (26)} = 6.25$, $p < 0.0001$ $t_{C,R\ (26)} = 4.05$, $p = 0.0004$ $t_{I,R\ (26)} = -2.21$, $p = 0.036$
	$FeCl_3$	0.53^{B}	
	River Plume	0.49^{C}	
> 20 um	Control	0.25^{A}	$t_{C,I\ (25)} = 8.15$, $p < 0.0001$ $t_{C,R\ (25)} = 4.00$, $p = 0.0005$ $t_{I,R\ =} 4.25$, $p = 0.0003$
	$FeCl_3$	0.56^{B}	
	River Plume	0.39^{C}	
< 5 µm	Control	0.35^{A}	$t_{C,I\ (26)} = 7.01$, $p < 0.0001$ $t_{C,R\ (26)} = 6.95$, $p < 0.0001$
	$FeCl_3$	0.46^{B}	
	River Plume	0.46^{B}	

Table 4. Results of Generalized Least Squares (GLS) Modeling. Bold p-values indicate significance at $\alpha = 0.10$. Tukey's pairwise contrasts ($\alpha = 0.10$) were run using treatment *slopes* where significant Treatment: Time interactions existed, or treatment *means* in the absence of significant Treatment: Time interactions. Letters in parentheses indicate groupings for each treatment (Control, $FeCl_3$, River Plume) based on pairwise contrasts.

		Treatment	**Time**	**Treatment: Time**
Fv/Fm	Total	$F_{2,24} = 19.01$ **p < 0.0001** *(A,B,C)*	$F_{1,24} = 0.68$ p= 0.42	$F_{2,24} = 0.28$ p= 0.75
	< 5 µm	$F_{2,24} = 31.00$ **p < 0.0001** *(A,B,B)*	$F_{1,24} = 2.00$ p= 0.17	$F_{2,24} = 0.40$ p= 0.67
	> 20 µm	$F_{2,23} = 31.14$ **p < 0.0001** *(A,B,C)*	$F_{1,23} = 0.046$ p= 0.83	$F_{2,23} = 0.62$ p= 0.55
FSC	*Synechococcus* sp.	$F_{2,24} = 35.44$ **p < 0.0001**	$F_{1,24} = 60.56$ **p < 0.0001**	$F_{2,24} = 7.83$ **p= 0.024** *(A,B,B)*
	Nano- and picoeukaryotes	$F_{2,24} = 4.77$ **p= 0.018** *(A,B,B)*	$F_{1,24} = 26.46$ **p < 0.0001**	$F_{2,24} = 1.94$ p= 0.16
Abundance	*Synechococcus* sp.	$F_{2,24} = 41.05$ **p < 0.0001**	$F_{1,24} = 223.20$ **p < 0.0001**	$F_{2,24} = 21.38$ **p < 0.0001** *(A,B,B)*
	Pico- and nanoeukaryotes*	$F_{2,114} = 0.80$ p= 0.45	$F_{1,114} = 81.06$ **p < 0.0001**	$F_{2,114} = 0.90$ p= 0.41
FL2	*Synechococcus* sp.	$F_{2,24} = 14.77$ **p= 0.0001** *(A,B,B)*	$F_{1,24} = 10.08$ **p= 0.0041**	$F_{2,24} = 0.91$ p= 0.42
FL3	Pico- and nanoeukaryotes	$F_{2,24} = 4.03$ **p= 0.031** *(A,B,B)*	$F_{1,24} = 12.34$ **p= 0.0018**	$F_{2,24} = 1.29$ p= 0.29
FL1 Ratio	*Synechococcus* sp.	$F_{2,23} = 1.48$ p= 0.25	$F_{1,23} = 1.41$ p= 0.25	$F_{2,23} = 0.08$ p= 0.92
	Pico- and nanoeukaryotes	$F_{2,24} = 3.18$ **p < 0.0001**	$F_{1,24} = 0.12$ p = 0.73	$F_{2,24} = 3.08$ **p= 0.064** *(A,B,AB)*

Table 5. Nutrient utilization and chlorophyll *a* net production efficiency (Δ Total Chlorophyll *a*: Δ dFe), estimated for the 0 h – 120 h time interval.

Treatment	$Si(OH)_4$: N	N: dFe	N: P	Total Chl. *a*: dFe
Control	0.83	1.85	6.23	0.62
$FeCl_3$	1.99	1.75	13.01	0.69
River Plume	1.47	4.48	10.64	1.05

Table 6. Synthesized results. The phytoplankton community response to the control, $FeCl_3$, and river plume iron sources are described for communities > 20 µm and < 20 µm. Phytoplankton < 20 µm are further differentiated into *Synechococcus* sp. and pico- and nanoeukaryotes. Italicized statements indicate changes in phytoplankton growth or physiology in direct response to iron addition.

Size Fraction	Synthesized Results
> 20 µm	1. *Net growth rate and final chlorophyll* a *2X to 5X higher in $FeCl_3$ than in other treatments* 2. *Rapid Fv/Fm increase after $FeCl_3$ addition; average Fv/Fm remained highest in $FeCl_3$ treatment* 3. *River plume iron source also increased Fv/Fm* 4. Diatom biomass at 120 h highest in $FeCl_3$ treatment 5. *Diatom composition similar in $FeCl_3$ and control treatments (*Pseudo-nitzschia *spp. dominant), while different in the river plume treatment (*Rhizosolenia *spp. dominant)*
< 20 µm	1. Net growth rate for cells 5- 20 µm similar across treatments 2. *Net growth rate for cells < 5 µm 3X higher in $FeCl_3$ and river plume treatments than in control* 3. *Fv/Fm higher in $FeCl_3$ and river plume treatments than in control* 4. *< 20 µm chlorophyll* a *comprised more of the total in river plume and control treatments*
Synechococcus sp.	1. $FeCl_3$ and river plume iron sources increased abundance to ~ 2X that of the control 2. *$FeCl_3$ and river plume iron sources increased cell size relative to control* 3. *Phycoerythrin per cell highest in $FeCl_3$ treatment, intermediate in river plume treatment* 4. No ROS response to any iron source
Pico- and Nanoeukaryotes	1. Abundance similar across all treatments; decreased 25 % over time 2. *Cells larger in $FeCl_3$ and river plume treatment; lowest in control treatment* 3. *Chlorophyll* a *per cell concentration higher in $FeCl_3$ and river plume treatments than in control* 4. *ROS production higher in control than in $FeCl_3$ or river plume treatments*

Table S1. Diatom shape and depth assumptions. The shape and depth assumption for every diatom taxon observed in settled samples is provided below. Exponents refer to references used to estimate the depth assumption for a given taxa. NOTE: The depth assumption is defined as cell depth: cell length. If a diatom was approximated as a lateral cylinder with a circular cross section, d=1 and no reference was used to estimate d.

Taxon	Shape Name	Depth Assumption (d)
Actinoptychus senarius	Circular Cylinder	0.5[1]
Asterionellopsis spp.	Cone	0.6[1]
Chaetoceros contortus	Chain of Lateral Cylinders	0.7[1]
Chaetoceros convolutus	Chain of Lateral Cylinders	0.7[1]
Chaetoceros danicus	Circular Cylinder	0.7[1]
Chaetoceros diadema	Chain of Lateral Cylinders	0.7[1]
Chaetoceros laciniosus	Chain of Lateral Cylinders	0.7[1]
Chaetoceros teres	Chain of Lateral Cylinders	0.7[1]
Corethron hystrix	Cylinder, Prolate Spheroid*	1[NA]
Coscinodiscus granii	Circular Cylinder	0.6[1]
Coscinodiscus marginatus	Circular Cylinder	0.6[1]
Cylindrotheca closterium	Prolate Spheroid	1[NA]
Ditylum brightwellii	Cylinder, Prolate Spheroid†	1 [NA]
Fragilariopsis pacifica	Elliptical Cylinder	0.1[2]
Leptocylindrus spp.	Chain of Lateral Cylinders	1 [NA]
Navicula spp.	Elliptical Cylinder	0.2[1]
Odontella spp.	Chain of Lateral Cylinders	1 [NA]
Paralia spp.	Chain of Lateral Cylinders	1 [NA]
Pleurosigma spp.	Elliptical Cylinder	0.7[3]
Pseudo-nitzschia delicatissima	Chain of Prolate Spheroids	0.9[1]
Pseudo-nitzschia multiseries	Chain of Prolate Spheroids	0.9[1]
Pseudo-nitzschia rotula	Chain of Prolate Spheroids	0.9[1]
Rhizosolenia spp.	Chain of Lateral Cylinders	1 [NA]
Skeletonema costatum	Chain of Lateral Cylinders	1 [NA]

Table S1 Continued…

Taxon	Shape Name	Depth Assumption (d)
Tabularia investiens	Elliptical Cylinder	0.6[4]
Thalassiosira rotula	Circular Cylinder	0.5[1]
Thalassiosira eccentrica	Circular Cylinder	0.5[1]
Thalassiosira gravida	Circular Cylinder	0.5[1]
Thalassiosira nordenskioeldii	Circular Cylinder	0.5[1]
Thalassiosira pacifica	Circular Cylinder	0.5[1]
Large *Thalassiosira* spp.	Circular Cylinder	0.5[1]
Small *Thalassiosira* spp.	Circular Cylinder	0.5[1]
Tropidoneis lepidoptera	Rectangular Box	0.4[4]
Misc. Diatom‡	Circular Cylinder	0.5[1]
Diatom B	Elliptical Cylinder	0.2[1]

[1]Ivanochko 2012; [2]Lundholm and Hasle 2010; Figure 63-74; 65 and 71; [3]Poulin et al. 2004; [4]Kaczmarska 2001

* A Cylinder and prolate spheroid shape was used to approximate the true shape of *Corethron hystrix*. Measurements were altered post-collection to more accurately approximate *Corethron* sp. as a cylinder with a half prolate spheroid on either end

†The cylinder and prolate spheroid shape was only used to measure *Ditylum brightwellii* to allow for three (measurements. Measurements were altered post-collection to approximate *Ditylum brightwellii* more accurately as a triangular prism.

‡ Diatom B was an unidentified “pill” shaped pennate diatom most similar to *Fragilariopsis* spp., though it was shorter and wider than *Fragilariopsis pacifica*

Table S2. Taxon-specific diatom biomass. Average biomass (ug L^{-1}) is provided for each diatom taxon observed in samples at the initial (0 h; n=3) and final (120 h; n=3) time points.

			Final					
	Initial	S.D.	Control	S.D	$FeCl_3$	S.D.	River	S.D.
Total Community	9.77	1.80	17.98	2.95	43.62	14.13	26.44	18.17
***Actinoptychus* spp.**	0.02	0.01	0.09	0.06	0.25	0.11	0.13	0.10
***Asterionella* spp.**	0.00	0.00	0.01	0.02	0.01	0.01	0.00	0.00
***Chaetoceros* spp.**	0.45	0.47	0.81	0.66	1.11	0.27	0.94	0.68
C. contortus	0.29	0.44	0.03	0.04	0.43	0.36	0.01	0.68
C. convolutus	0.11	0.03	0.68	0.59	0.58	0.48	0.54	0.71
C. danica	0.01	0.01	0.01	0.02	0.07	0.08	0.03	0.06
C. diadema	0.00	0.00	0.05	0.05	0.00	0.00	0.03	0.05
C. laciniosus	0.02	0.02	0.01	0.02	0.00	0.00	0.15	0.18
C. teres	0.02	0.03	0.02	0.02	0.02	0.04	0.14	0.11
***Corethron* spp.**	2.93	0.32	3.31	1.73	5.33	6.22	4.22	2.32
***Coscinodiscus* spp.**	1.07	0.98	0.43	0.49	0.35	0.61	0.54	0.83
C. granii	0.06	0.10	0.43	0.49	0.35	0.61	0.19	0.22
C. marginatus	1.01	0.88	0.00	0.00	0.00	0.00	0.35	0.61
C. closterium	0.01	0.01	0.08	0.03	0.22	0.06	0.19	0.13
D. brightwellii	0.00	0.00	0.00	0.00	0.00	0.00	0.01	0.01
F. pacifica	0.00	0.00	0.00	0.00	0.00	0.00	0.00	0.00
***Leptocylindrus* spp.**	0.09	0.12	0.65	1.06	0.77	0.63	1.70	2.65
***Navicula* spp.**	0.00	0.01	0.00	0.01	0.48	0.81	0.01	0.01
***Odontella* spp.**	0.00	0.00	0.03	0.03	0.00	0.00	0.00	0.00
***Paralia* spp.**	0.01	0.01	0.00	0.00	0.08	0.14	0.72	1.25
***Pleurosigma* spp.**	0.00	0.00	0.01	0.01	0.23	0.39	0.01	0.02
***Pseudo-nitzschia* spp.**	0.46	0.04	4.49	0.85	18.86	3.81	2.96	0.89
P. delicatissima	0.03	0.01	0.20	0.01	2.76	2.83	0.20	0.18
P. multiseries	0.42	0.02	4.07	0.80	14.96	6.64	2.08	0.11
P. rotula	0.02	0.01	0.22	0.08	1.10	0.38	0.68	0.61
***Rhizoselenia* spp.**	3.28	2.32	1.28	0.89	4.88	4.54	11.14	13.28
> 100 µm	3.12	2.40	1.23	0.88	4.78	4.62	7.79	10.92
< 100 µm	0.16	0.21	0.05	0.03	0.10	0.18	3.35	2.38
S. costatum	0.07	0.06	0.40	0.32	0.60	0.36	0.47	0.40
T. investiens	0.01	0.01	0.00	0.00	0.00	0.01	0.00	0.00
***Thalassiosira* spp.**	0.83	0.38	3.66	1.33	6.82	1.21	2.72	1.55
T. rotula	0.02	0.02	0.17	0.21	0.12	0.12	0.05	0.06
T. eccentrica	0.50	0.46	2.01	0.49	3.22	0.53	0.80	0.33
T. gravida	0.00	0.00	0.00	0.00	0.22	0.38	0.00	0.00
T. nordenskioeldii	0.00	0.00	0.09	0.10	0.16	0.15	0.01	0.02
T. pacifica	0.20	0.07	0.69	0.87	1.14	0.39	0.44	0.30
Large Thalassiosira	0.00	0.00	0.00	0.00	0.02	0.03	0.02	0.02
Small Thalassiosira	0.10	0.02	0.72	0.11	1.92	0.70	1.32	1.47
Misc. Diatom	0.05	0.08	0.00	0.00	0.00	0.00	0.00	0.00
Diatom b	0.00	0.00	0.00	0.01	0.00	0.00	0.00	0.00
T. lepidoptera	0.48	0.40	2.73	1.26	2.46	1.85	0.69	0.49

Table S3. Taxon-specific diatom abundance. Average diatom concentration (cells L^{-1}) is provided for each diatom taxon observed in samples at the initial (0 h; n=3) and final (120 h; n=3) time points.

			Final					
	Initial	S.D.	Control	S.D	$FeCl_3$	S.D.	River	S.D.
Total Community	26,639	5,206	126,085	31,893	564,316	97,544	150,967	29,345
***Actinoptychus* spp.**	249	207	1,066	732	3,053	1,479	1,967	782
***Asterionella* spp.**	45	39	48	84	113	196	0	0
***Chaetoceros* spp.**	1,063	171	3,392	588	7,236	783	5,778	1,001
C. contortus	158	39	388	303	3,166	2,500	68	118
C. convolutus	611	68	1,841	968	3,392	1,223	3,132	231
C. danica	68	68	48	84	339	339	452	518
C. diadema	23	39	242	222	0	0	68	118
C. laciniosus	113	141	97	168	0	0	882	1,044
C. teres	113	196	97	84	339	588	1,063	274
***Corethron* spp.**	950	118	1,260	550	1,696	1,795	2,058	645
***Coscinodiscus* spp.**	136	68	97	84	113	196	384	409
C. granii	23	39	97	84	113	196	317	306
C. marginatus	113	39	0	0	0	0	68	118
C. closterium	520	104	1,551	801	4,297	1,603	5,744	2,981
D. brightwellii	0	0	0	0	0	0	34	59
F. pacifica	226	78	242	168	0	0	452	783
***Leptocylindrus* spp.**	724	341	1,163	291	4,070	6,171	2,861	3,104
***Navicula* spp.**	90	104	97	168	452	392	181	171
***Odontella* spp.**	0	0	48	84	0	0	0	0
***Paralia* spp.**	68	118	0	0	452	783	916	1,586
***Pleurosigma* spp.**	23	39	48	84	113	196	113	196
***Pseudo-nitzschia* spp.**	14,473	2,308	102,051	43,722	492,179	96,454	49,953	9,000
P. delicatissima	1,945	659	12,357	2,340	126,182	81,756	7,892	7,499
P. multiseries	11,985	2,181	84,800	38,243	335,017	176,959	32,009	8,804
P. rotula	520	282	4,894	3,987	30,980	5,302	10,052	9,399
***Rhizoselenia* spp.**	2,058	652	1,502	888	2,714	2,446	52,135	38,576
> 100 µm	837	481	533	550	1,244	706	4,308	6,026
< 100 µm	1,199	553	969	366	1,470	2,546	47,827	32,643
S. costatum	1,153	1,658	4,943	634	6,671	5,259	5,800	5,443
T. investiens	226	104	145	0	0	0	0	0
***Thalassiosira* spp.**	3,957	577	13,520	2,035	38,443	9,260	21,811	1,055
T. rotula	158	171	194	84	678	897	294	348
T. eccentrica	565	196	1,308	145	3,731	897	1,809	196
T. gravida	0	0	0	0	565	979	0	0
T. nordenskioeldii	23	39	339	303	791	196	407	538
T. pacifica	769	78	2,181	1,098	3,957	783	2,793	901
Large Thalassiosira	0	0	0	0	113	196	181	171
Small Thalassiosira	2,442	413	9,498	1,021	28,606	8,590	16,327	875
Misc. Diatom	23	39	0	0	0	0	0	0
Diatom b	226	141	145	0	113	196	226	392
T. lepidoptera	407	179	1,599	145	2,261	1,371	848	449

Table S4. Daily nutrient utilization ratios and growth efficiencies. Utilization ratios and phytoplankton growth efficiency, with respect to dFe, for each time interval are provided for each treatment. Note: Growth efficiency was not calculated for time intervals in which total chlorophyll *a* decreased.

Treatment	Time Interval (Hour)	$Si(OH)_4$: N	N: dFe	N: P	Total Chl. *a*: dFe
Control	0-48	1.16	1.00	2.93	NA
	48-72	0.73	2.71	26.87	1.91
	72-96	8.26	1.60	84.91	0.72
	96-120	4.37	2.28	7.07	0.54
$FeCl_3$	0-48	0.50	0.31	1.35	0.11
	48-72	2.01	1.26	13.43	1.59
	72-96	1.47	14.14	14.09	12.39
	96-120	13.11	0.63	2.00	NA
River Plume	0-48	1.62	1.22	10.39	0.15
	48-72	1.71	9.37	11.32	5.37
	72-96	1.14	19.40	14.71	9.40
	96-120	1.40	12.74	6.52	4.10

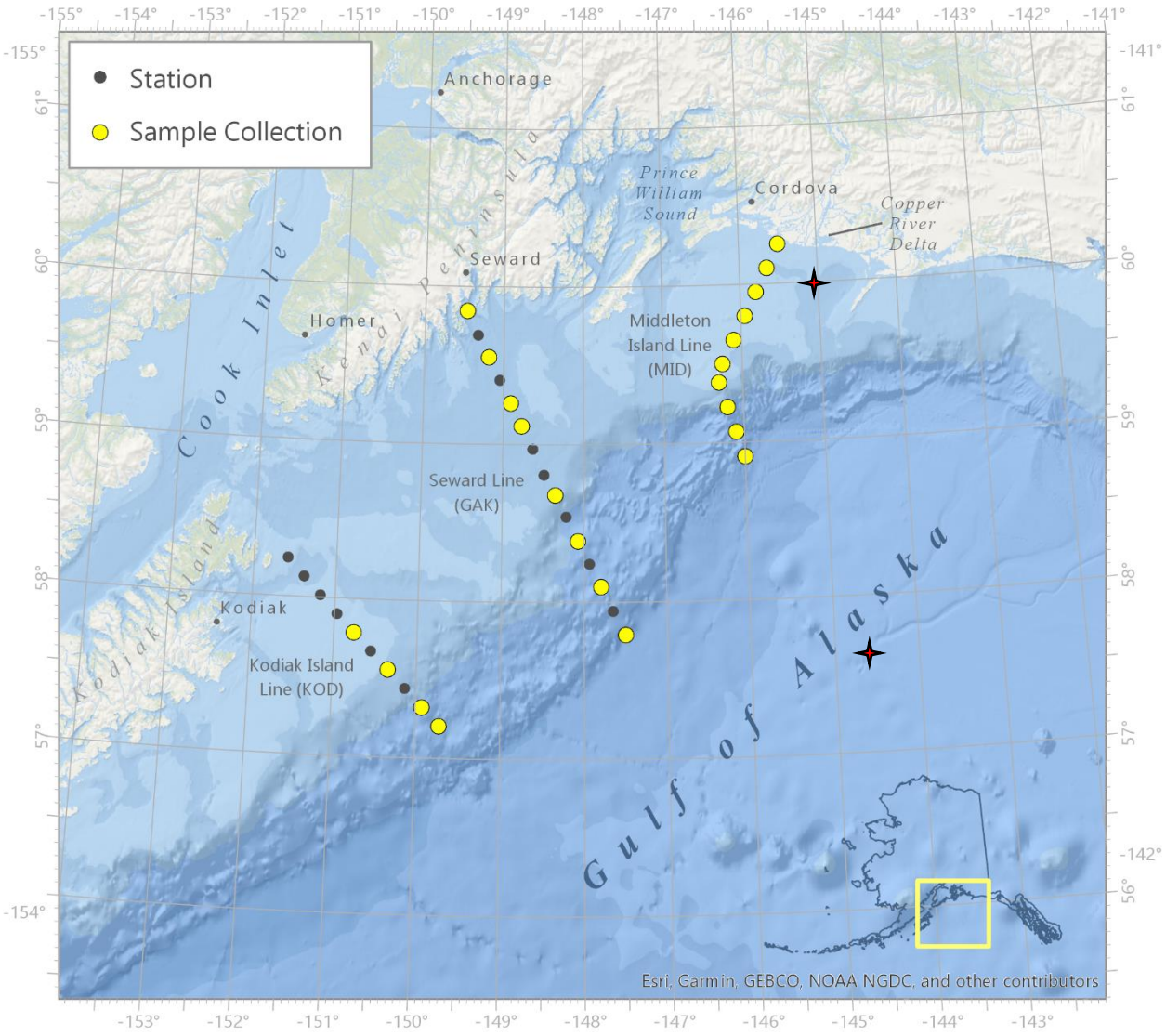

Figure 1. NGA LTER study site. Three transects comprise the NGA LTER study site. The site extends from just west of the Copper River Delta to the west of Cook Inlet (Kodiak Island Line) and from 10 nmi to 150 nm offshore to cover an area roughly 2.3 x 10^5 km^2. Note: Stations are identified numerically (e.g. GAK 1) based on distance offshore. Water for the iron addition experiment was sourced from the Copper River Plume and the HNLC region (red stars). Ambient phytoplankton communities from stations indicated by yellow symbols were used to contextualize the iron addition experiment within the NGA.

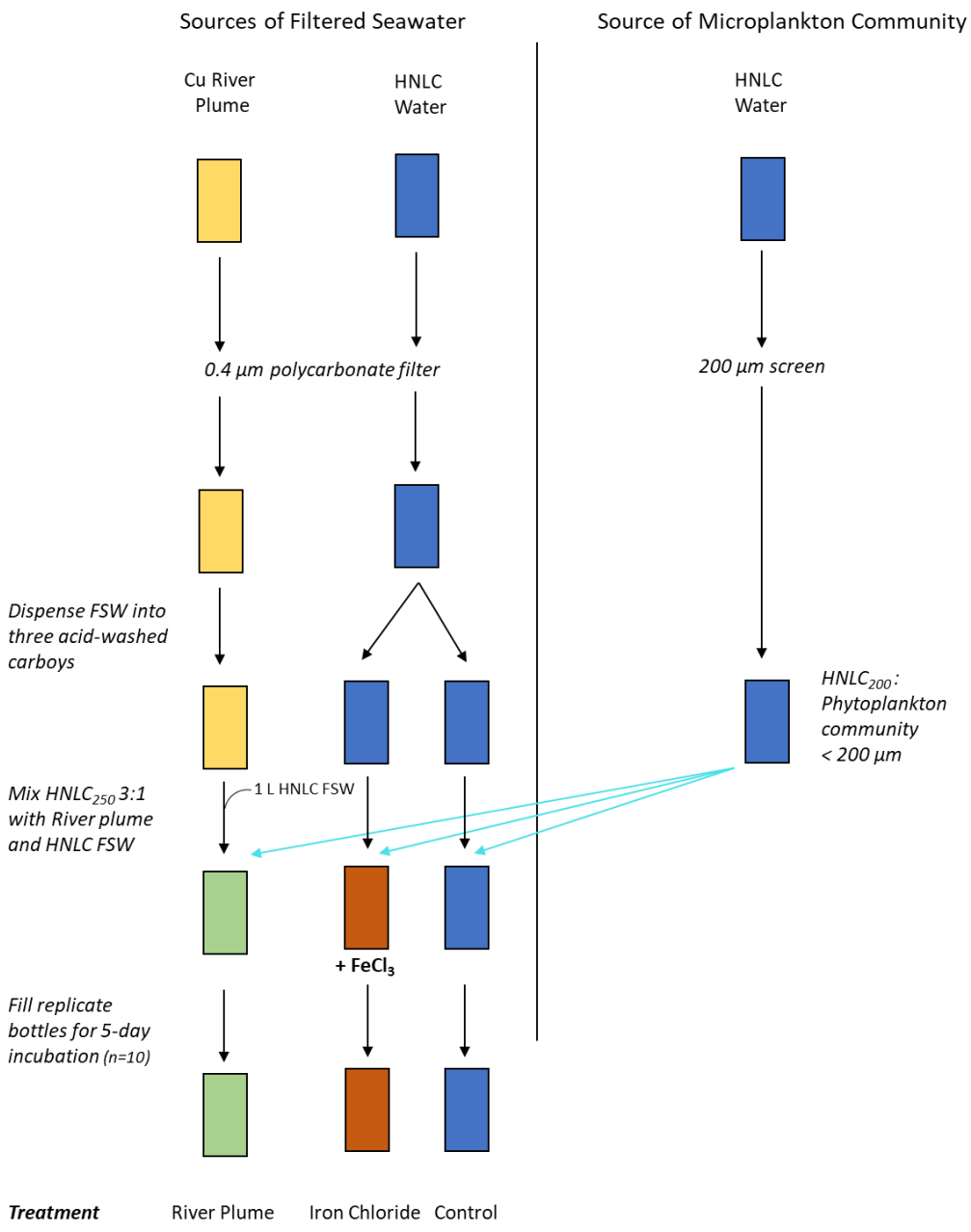

Figure 2. Schematic of iron addition experiment setup. Note only one replicate per treatment is shown, though ten bottles per treatment were sampled during the course of the experiment.

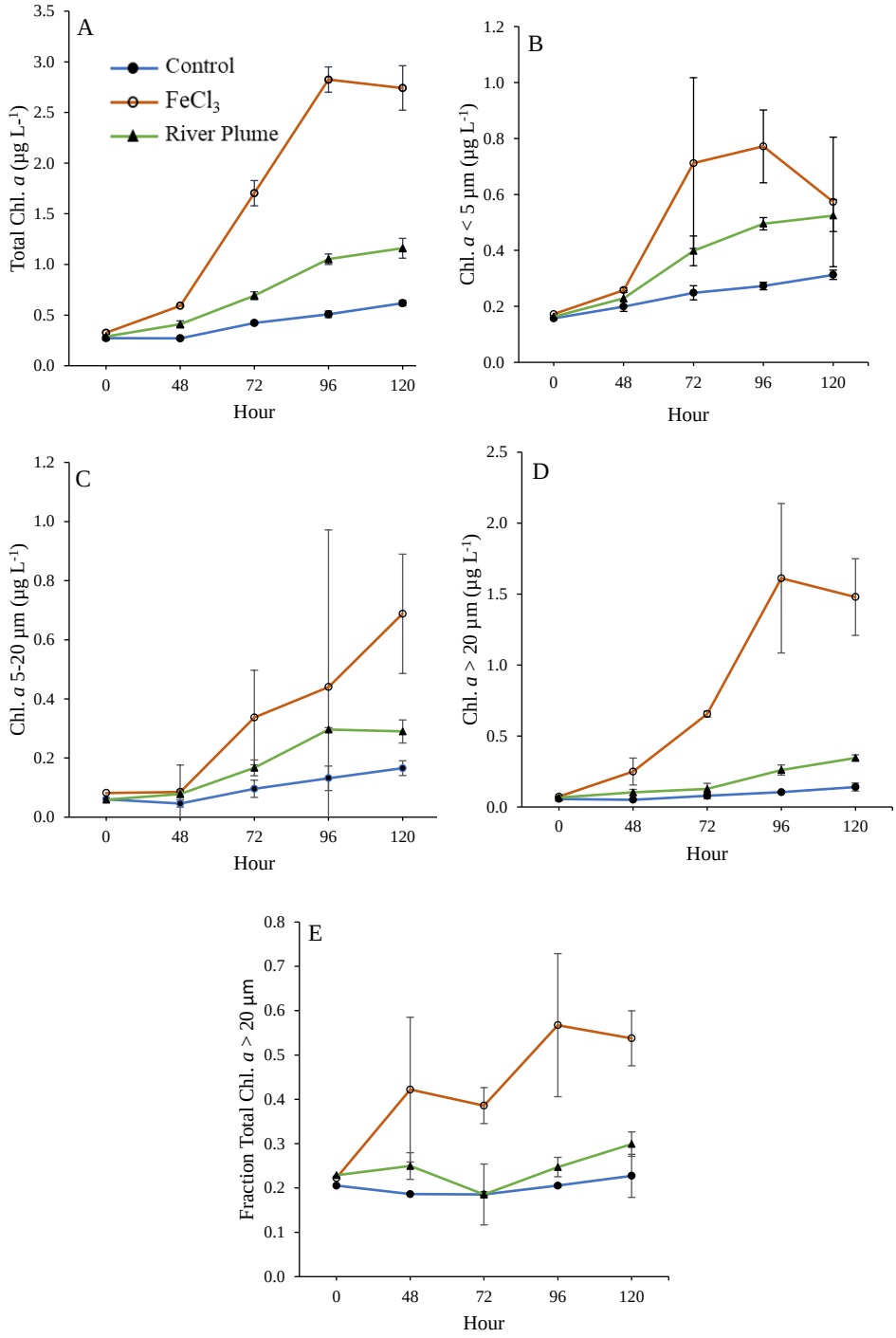

Figure 3. Changes in size-fractionated chlorophyll *a* concentrations (A, Total; B, < 5 µm; C, 5-20 µm; D, > 20 µm; E, Fraction of total chlorophyll *a* > 20 µm) in control and iron addition treatments. Points represent mean ± 1 standard deviation and in some cases are smaller than the graphed point. Note different y-axis scales between size-fractions.

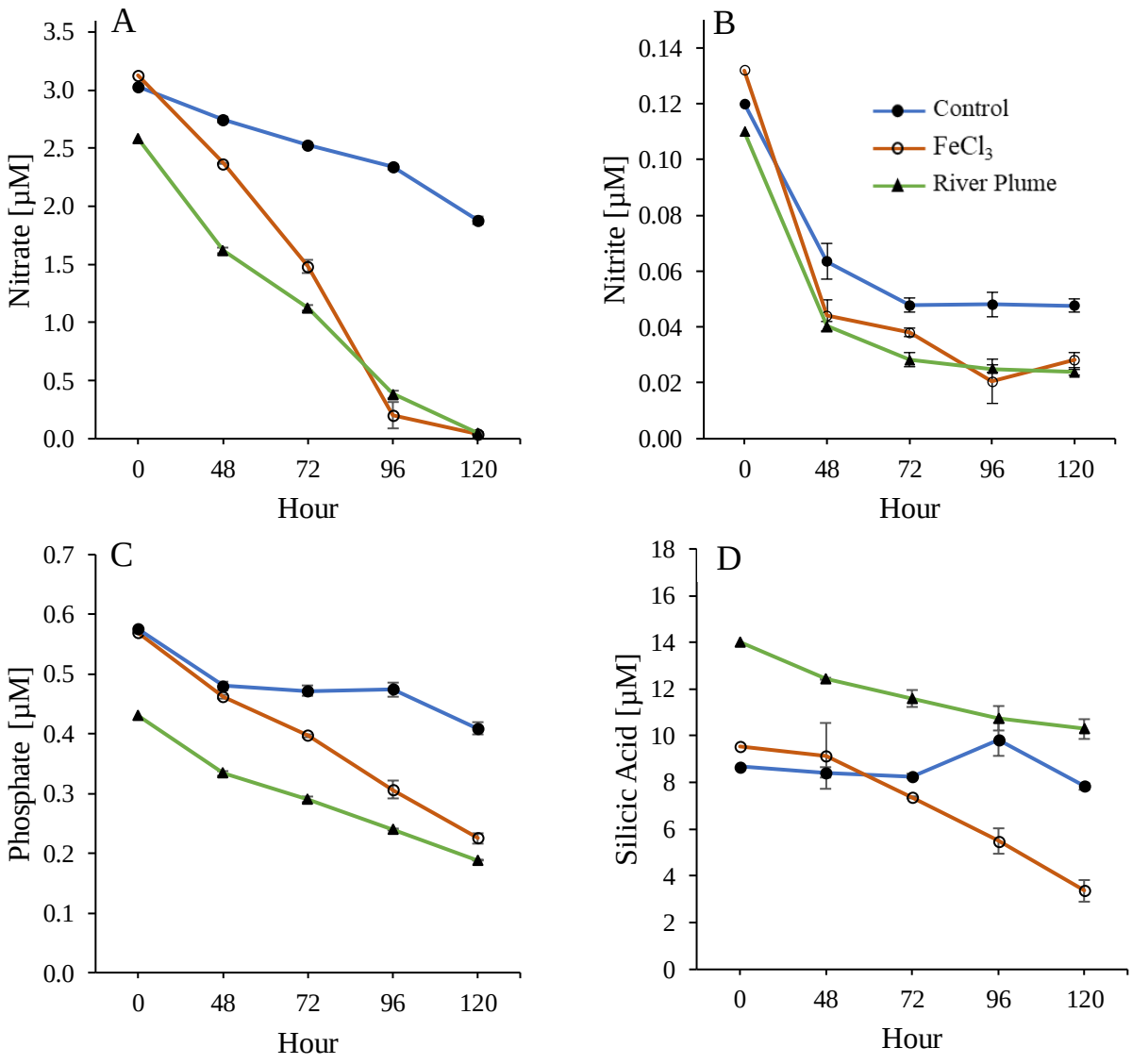

Figure 4. Changes in macronutrient (A, Nitrate; B, Nitrite; C, Phosphate; D, Silicic Acid) in control and iron addition treatments. Values represent the average of experimental bottles (n= 1 at Hour 0; n= 2 at Hours 48-96; n= 3 at Hour 120). Error bars represent ±1 standard deviation and are smaller than plotted points in some cases.

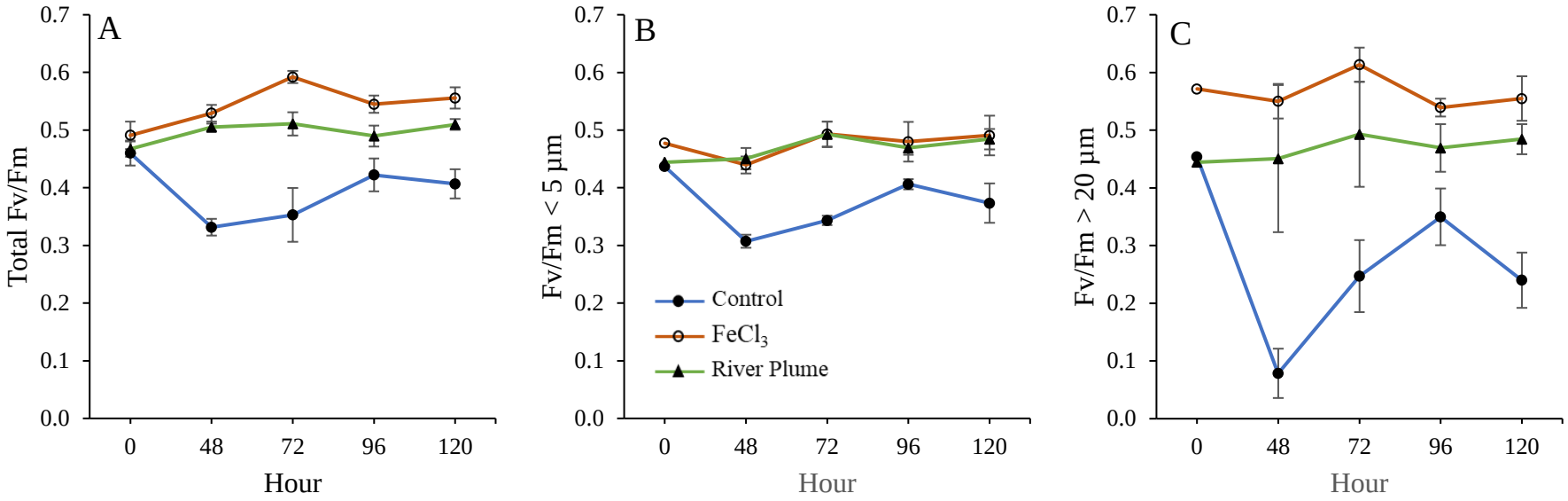

Figure 5. Mean Fv/Fm for cells of different sizes (A, Total; B, < 5 µm; C, > 20 µm) in control and iron addition treatments. Values represent the average of experimental bottles (n= 1 at Hour 0; n= 2 at Hours 48-96; n= 3 at Hour 120). Error bars represent ±1 standard deviation and are smaller than plotted points in some cases.

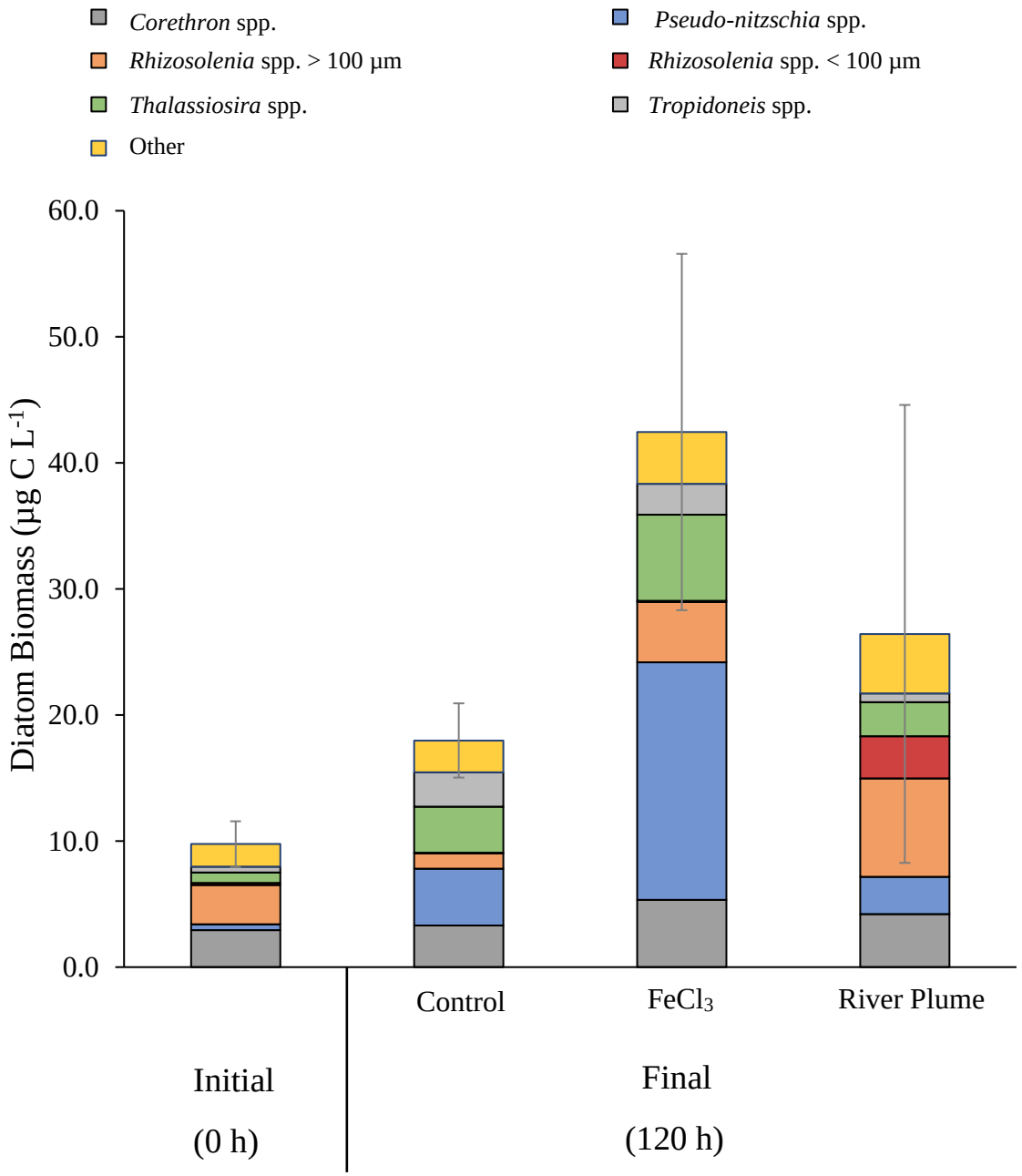

Figure 6. Taxon-specific changes in diatom biomass for control and iron addition treatments at initial (0 h) and final (120 h) time points. Values represent averages of replicate bottles (n =3); error bars represent ± 1 standard deviation for *total diatom biomass*.

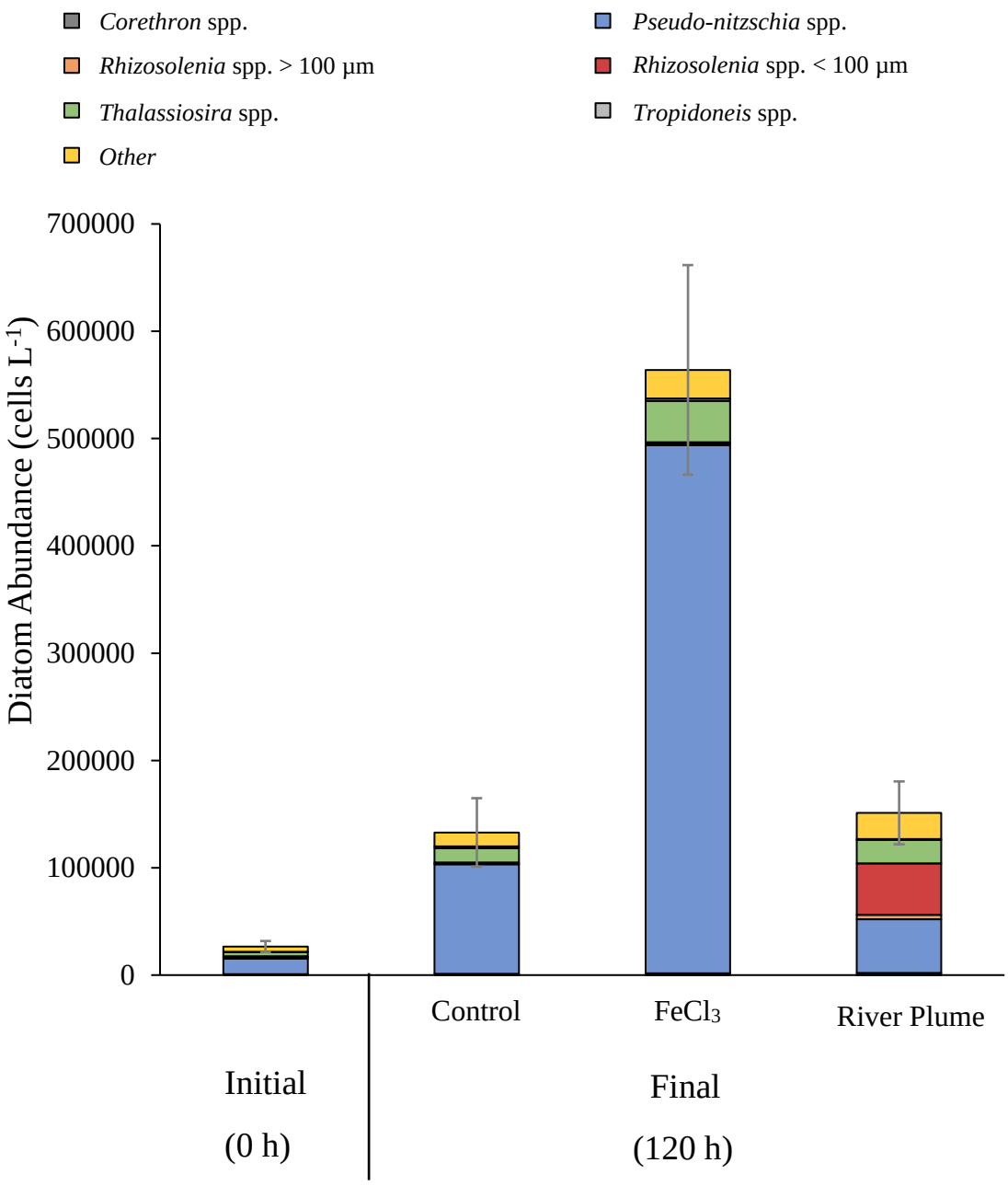

Figure 7. Taxon-specific changes in diatom abundance for control and iron addition treatments at initial (0 h) and final (120 h) time points. Values represent averages of replicate bottles (n= 3); error bars represent ± 1 standard deviation for *total diatom abundance*.

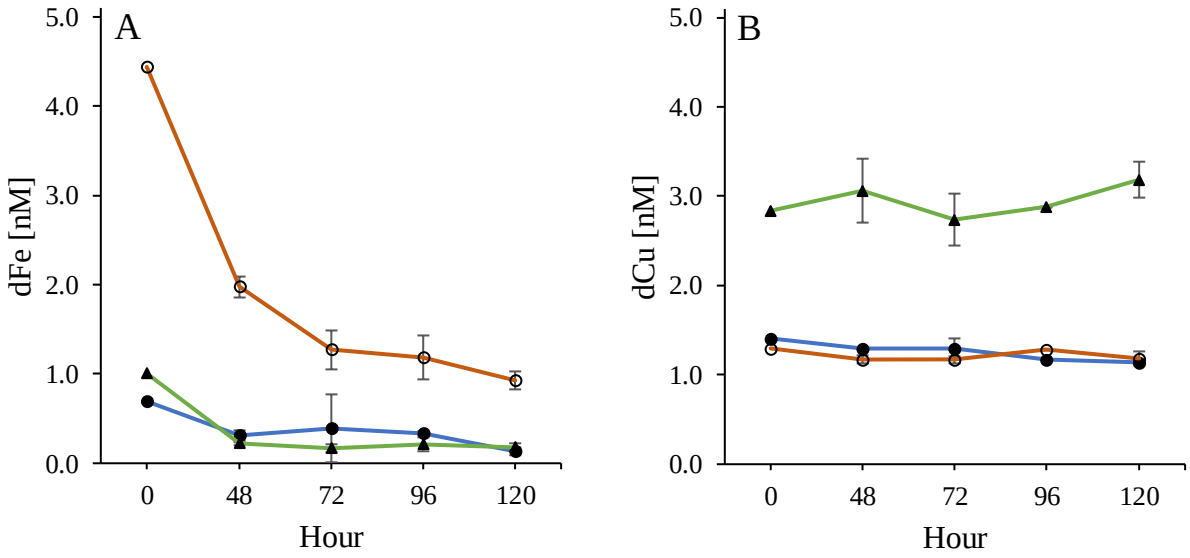

Figure 8. Changes in dFe and dCu concentrations in control and iron addition treatments. Values represent the average of experimental bottles (n= 1 at 0 h; n= 2 at Hours 48- 96 h; n= 3 at 120 h). Error bars represent ±1 standard deviation and are smaller than plotted points in some cases.

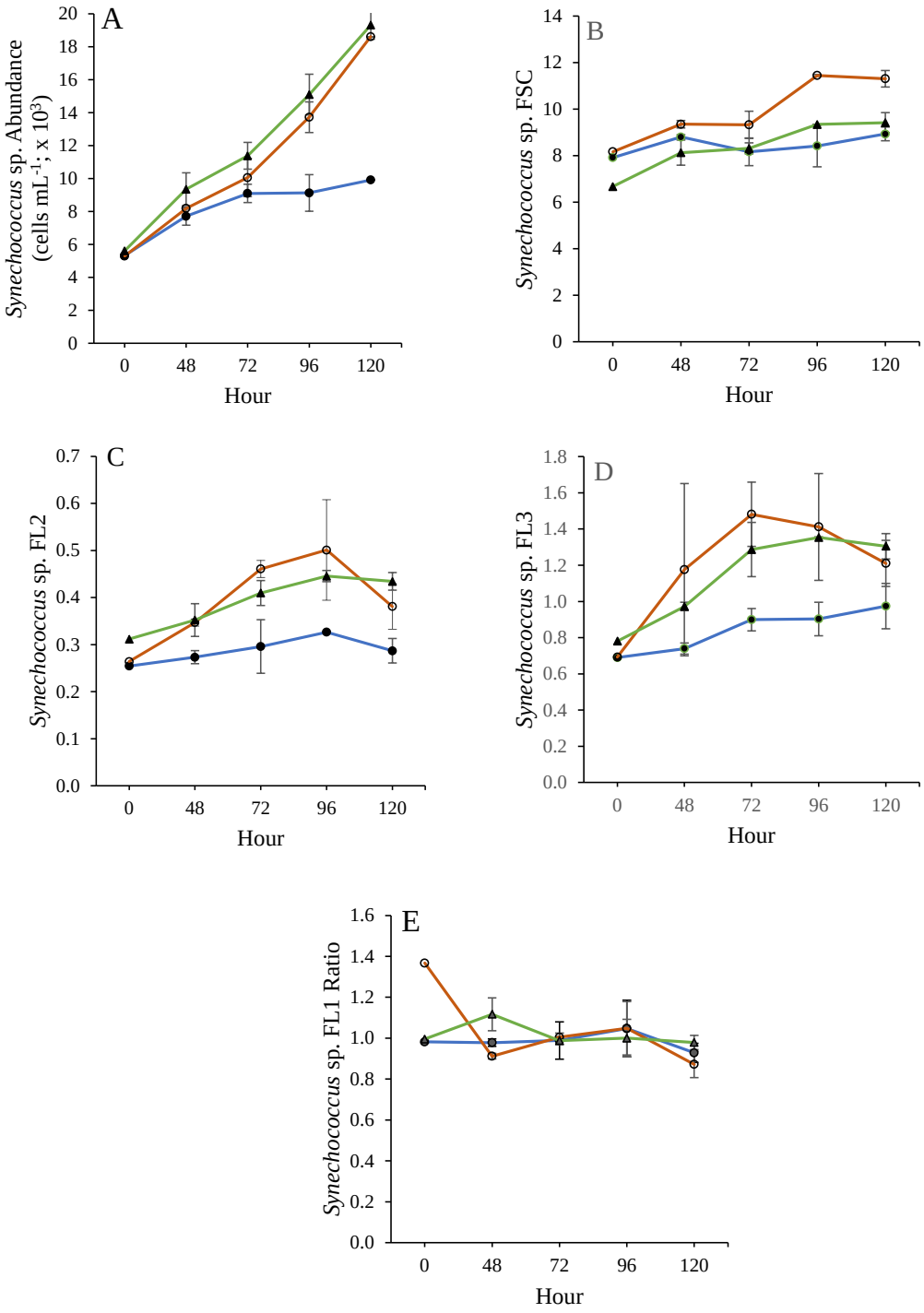

Figure 9. Flow cytometric measurements (A, Abundance; B, Forward Scatter; C, Yellow-orange fluorescence (FL2); D, Red fluorescence (FL3); E, Green fluorescence (FL1 ratio)) of *Synechococcus* sp. in control and iron addition treatments. Values represent the average of experimental bottles (n= 1 at Hour 0; n= 2 at Hours 48-96; n= 3 at Hour 120). Error bars represent ±1 standard deviation and are smaller than plotted points in some cases. Note different y-axis scales across measurements.

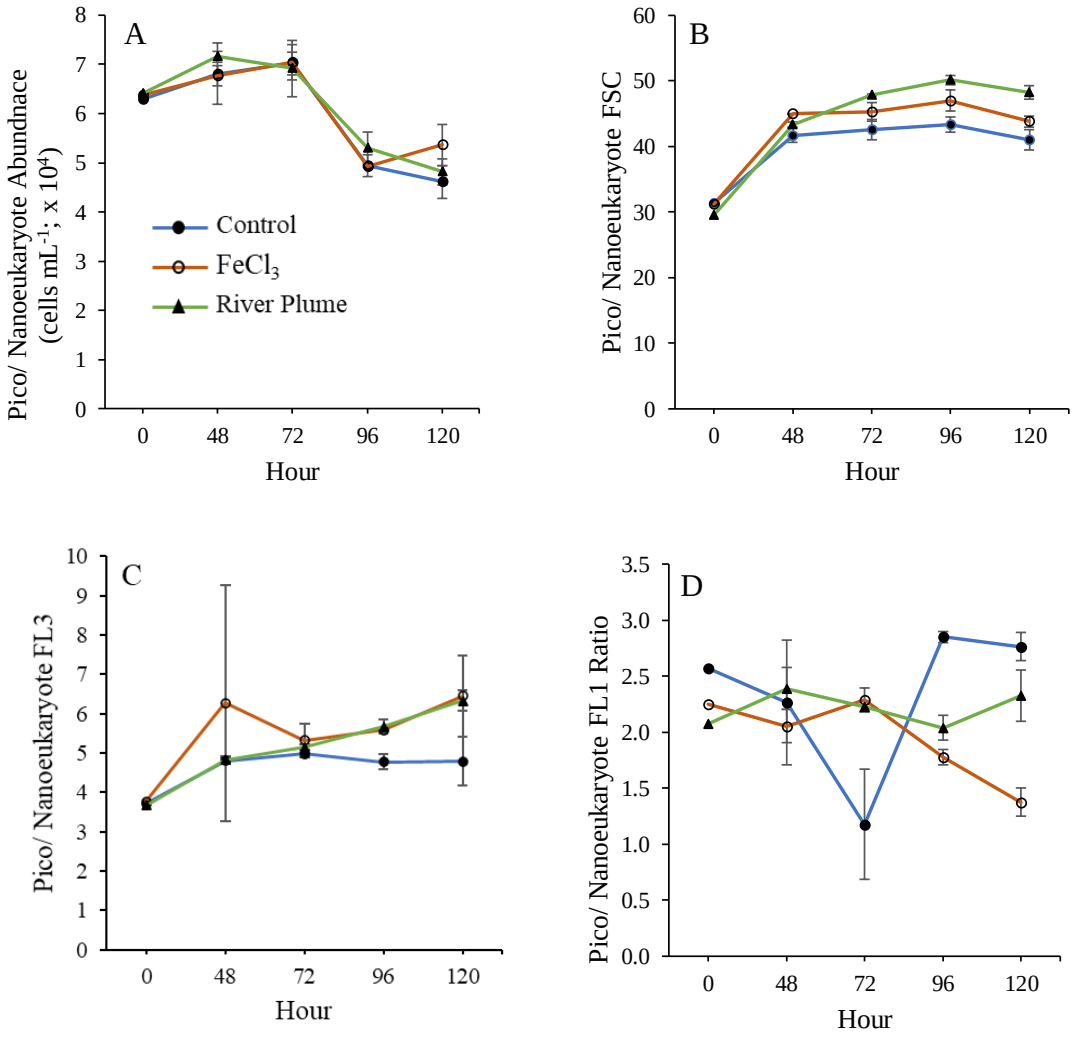

Figure 10. Flow cytometric measurements (A, Abundance; B, Forward Scatter; C, Red Fluorescence (FL3); D, Green fluorescence (FL1 ratio)) for pico- and nanoeukaryotes in control and iron addition treatments. Values represent the average of experimental bottles (n= 1 at 0 h; n= 2 at 49- 96 h; n= 3 at 120 h). Error bars represent ±1 standard deviation and are smaller than plotted points in some cases. Note different y-axis scales across measurements.

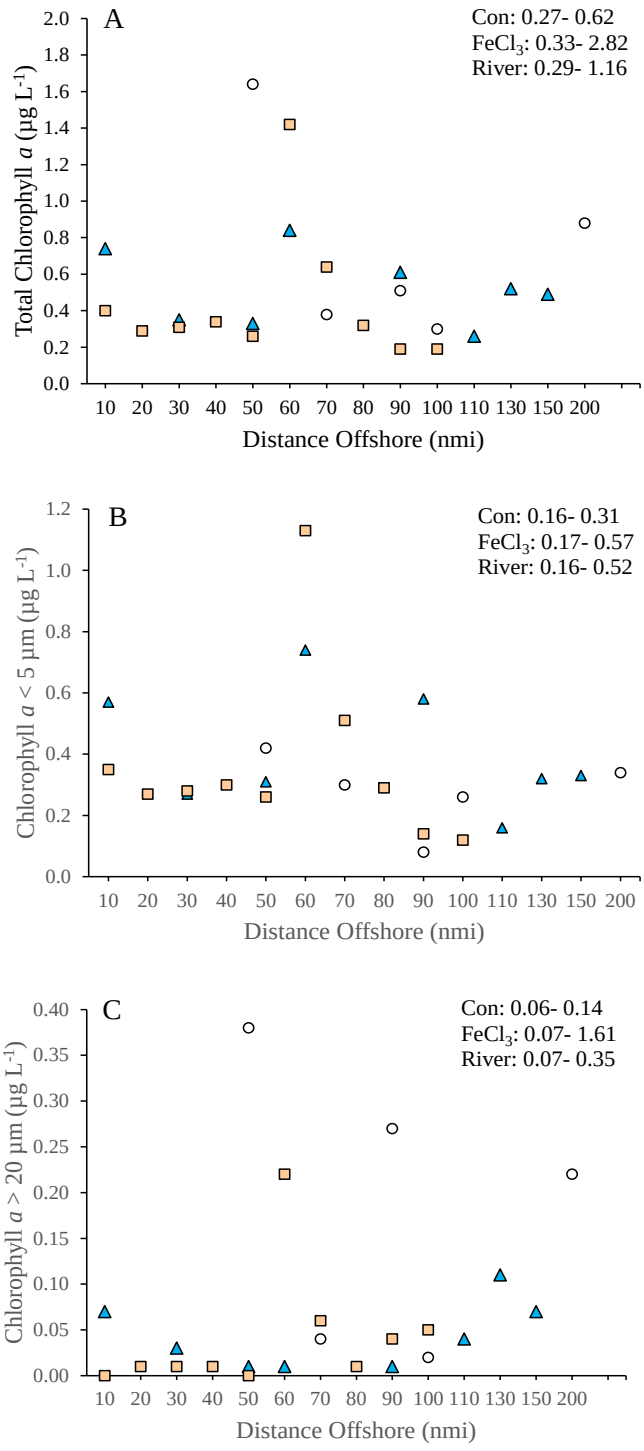

Figure 11. Size-fractionated chlorophyll *a* concentrations (A, Total; B, < 5 µm; C, > 20 µm) measured for ambient phytoplankton communities on LTER transects at 0 m. Ranges of chlorophyll *a* measured in iron addition treatments are provided to facilitate intercomparison of experimental and ambient phytoplankton communities. Note different y-axis scales across size fractions.

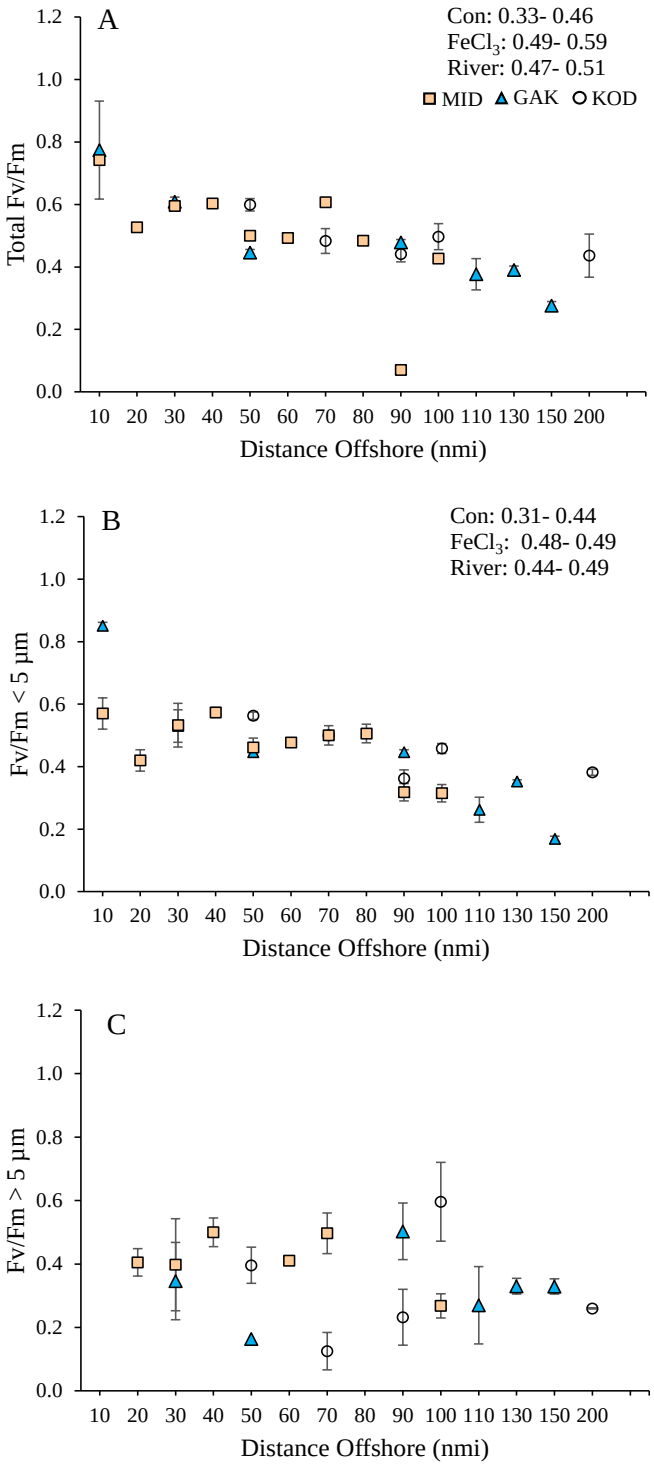

Figure 12. Size-fractionated Fv/Fm (A, Total; B, < 5 µm; C, > 5 µm) measured for ambient phytoplankton communities on LTER transects at 0 m. Values represent mean ± 1 sd for triplicate subsamples. Where appropriate, ranges of Fv/Fm values measured in iron addition treatments are provided to facilitate the intercomparison of experimental and ambient phytoplankton communities.

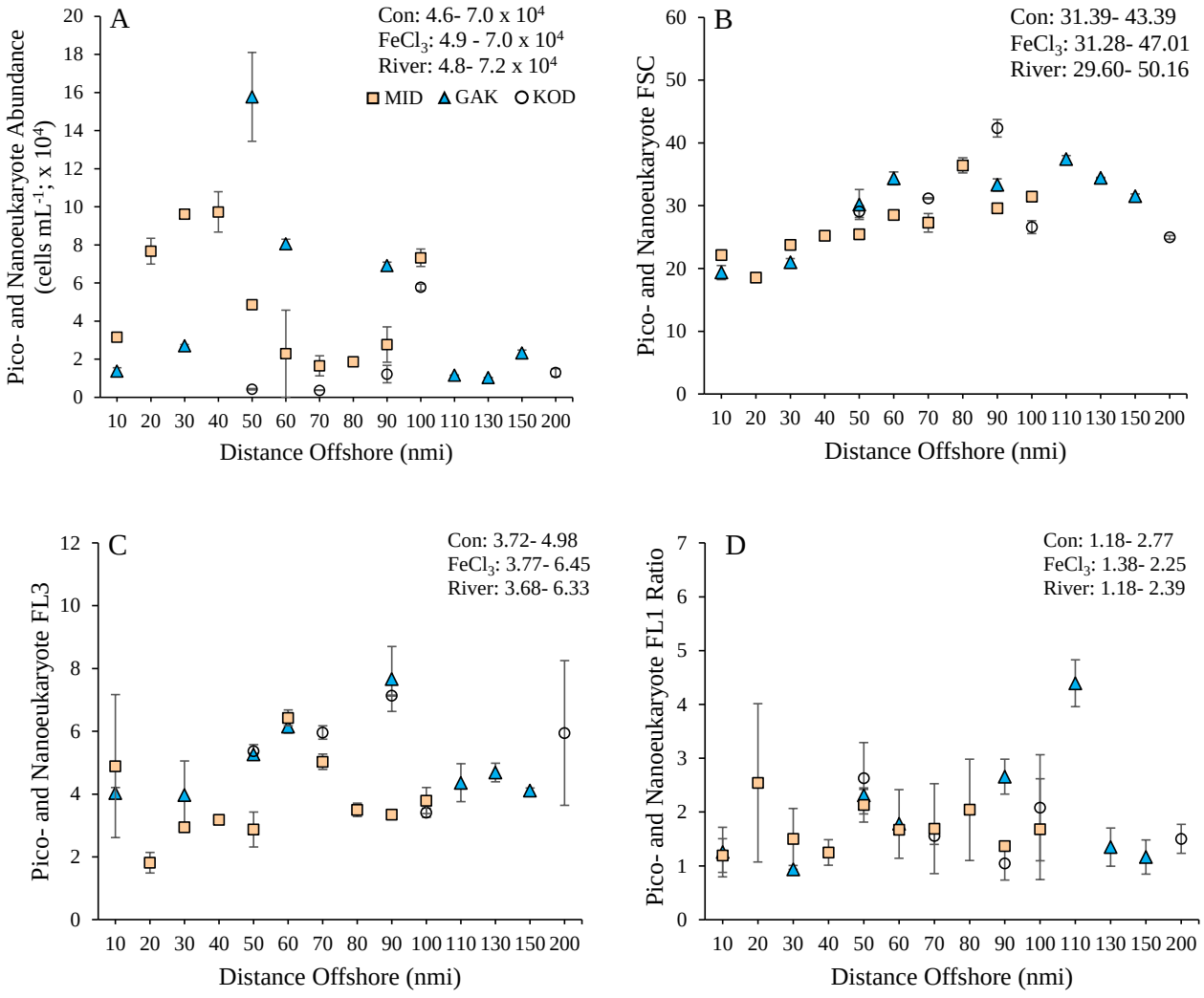

Figure 13. Flow cytometric properties (A, Abundance; B, FSC; C, FL3; D, FL1 ratio) for pico- and nanoeukaryotes on LTER transects sampled at 0 m. Values represent mean ± 1 standard deviation of duplicate samples. Ranges of each property measured in iron addition treatments are provided to facilitate intercomparison of experimental and ambient phytoplankton communities. Note different y-axes across properties. Note different y-axis scales across properties.

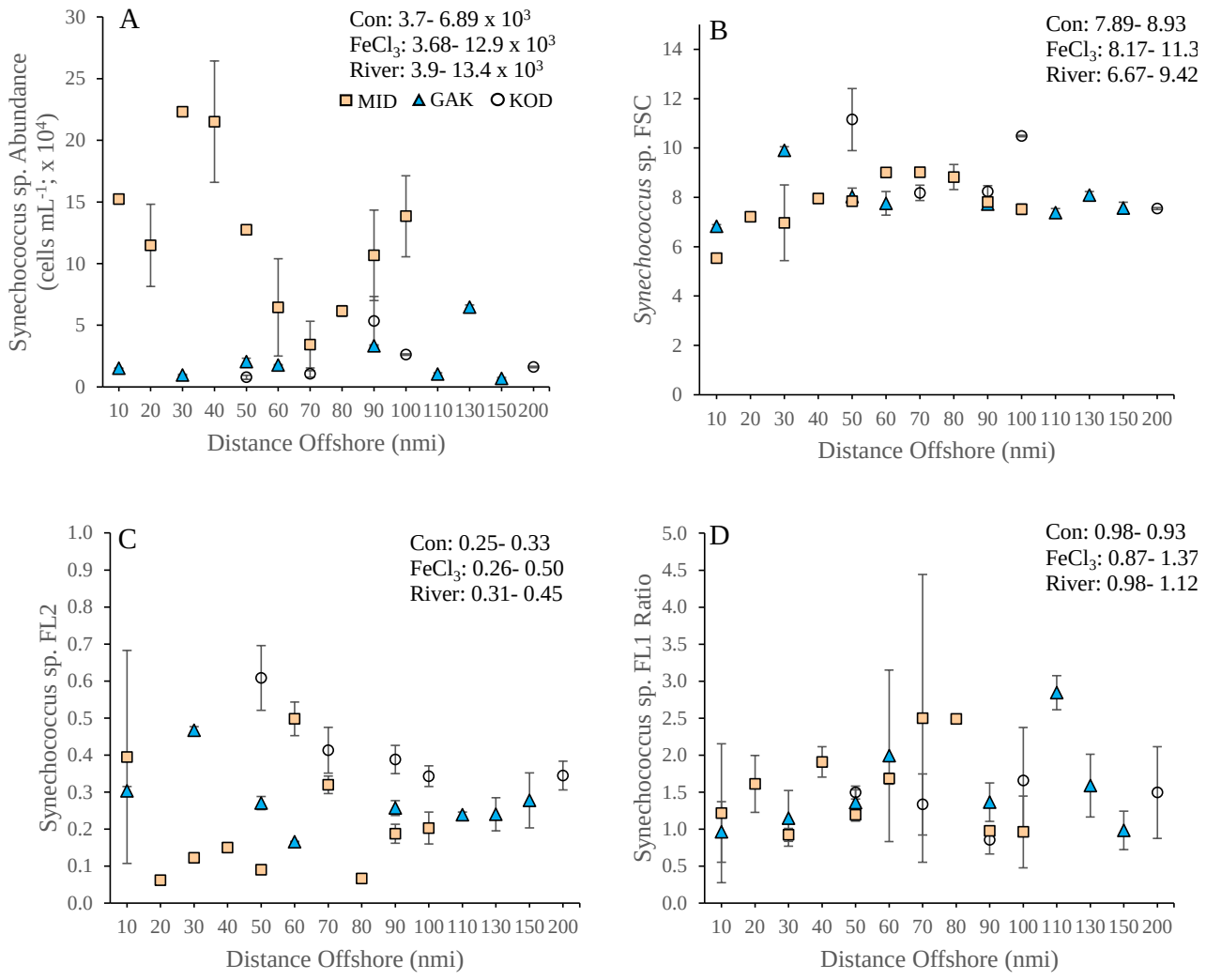

Figure 14. Flow cytometric properties (A, Abundance; B, FSC; C, FL3; D, FL1 ratio) for *Synechococcus* sp. on LTER transects sampled at 0 m. Values represent mean ± 1 standard deviation of duplicate samples. Ranges of each property measured in iron addition treatments are provided to facilitate intercomparison of experimental and ambient phytoplankton communities. Note different y-axes across properties. Note different y-axis scales across properties.

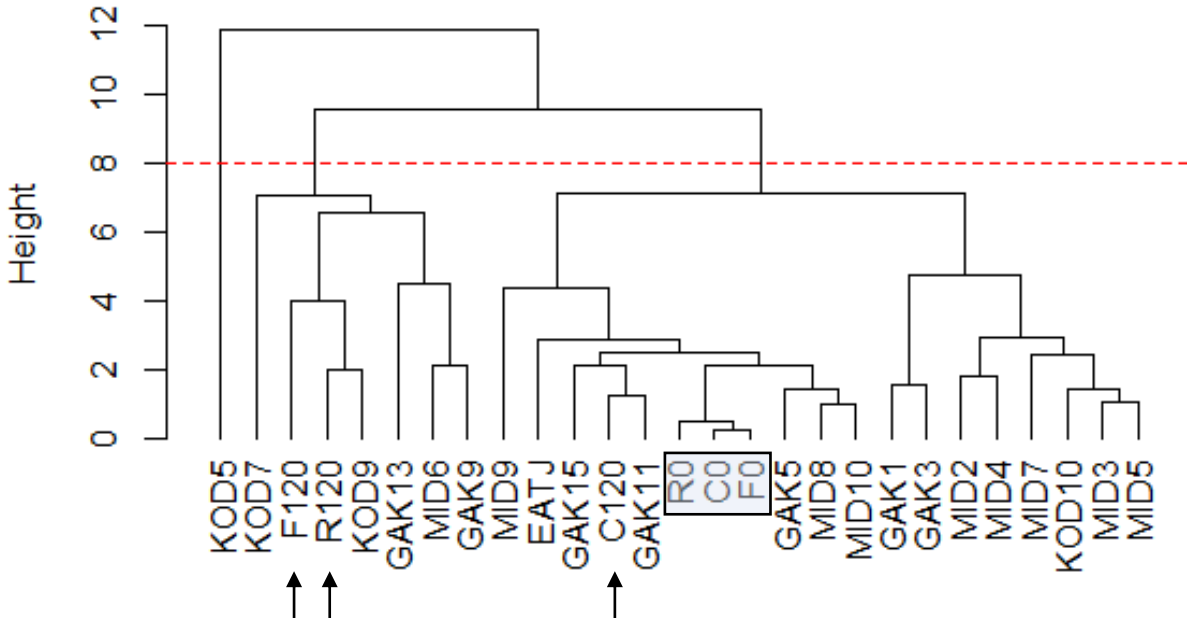

Figure 15. Clustering results of iron addition experiment samples within NGA LTER samples. Labels on the x-axis indicate specific LTER stations that were sampled during the July 2019 process cruise. The blue rectangle emphasizes the cluster of initial iron addition experiment samples (0 h; C: Control; F: $FeCl_3$; R: River plume). Arrows note the position of iron addition experiment samples at the final time point (120 h). The red dotted line represents approximate delineation of three regional groups, determined by K-Means analysis.

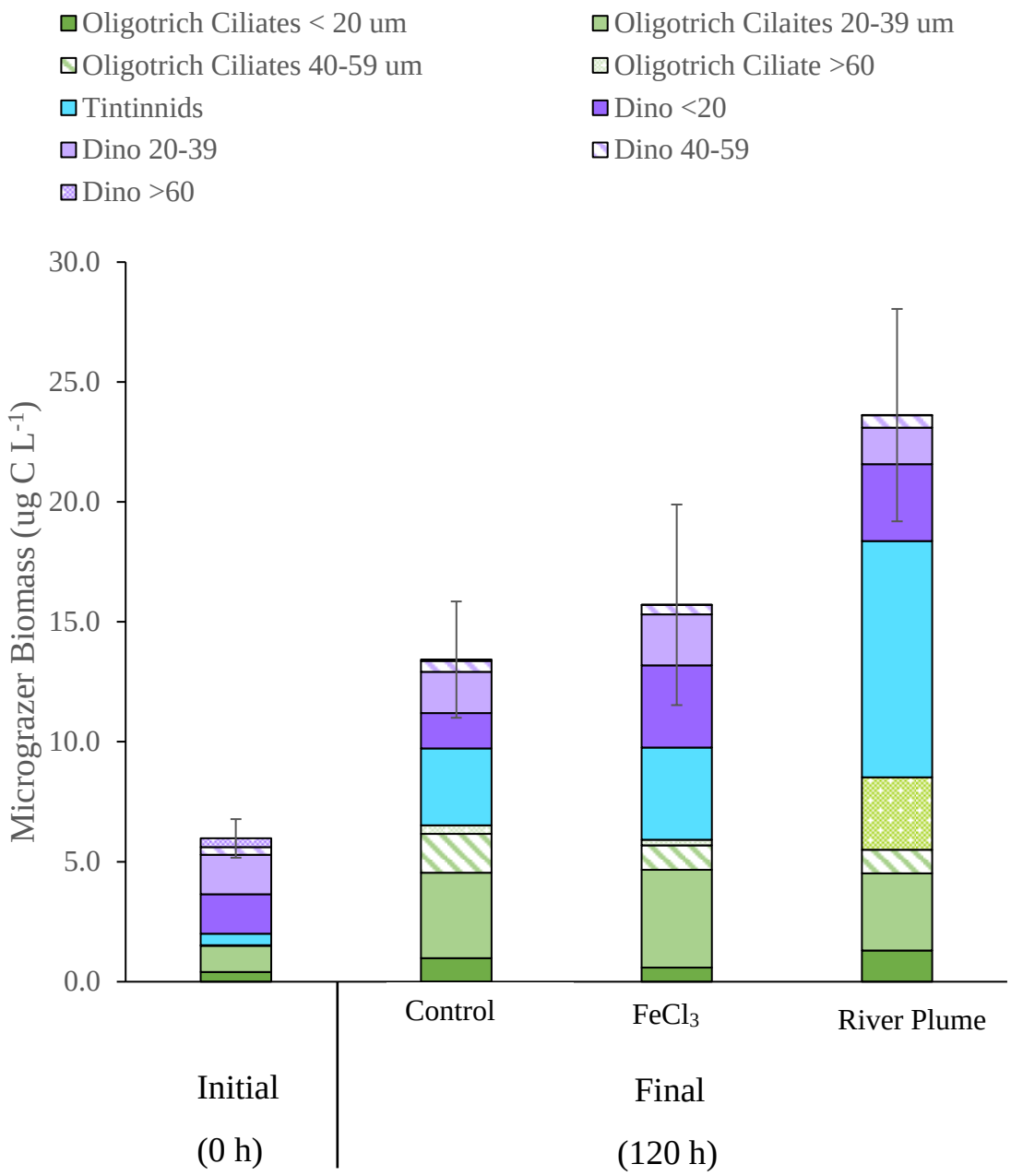

Figure 16. Size-specific changes in micrograzer abundance for control and iron addition treatments at initial (0 h) and final (120 h) time points. Values represent averages of replicate bottles (n= 3). Error bars represent ± 1 standard deviation for *total micrograzer biomass*. Note: Micrograzer biomass estimates were obtained from Lugol's preserved samples counted by Celia Ross (Strom Lab) and were not directly part of this thesis' sampling effort.

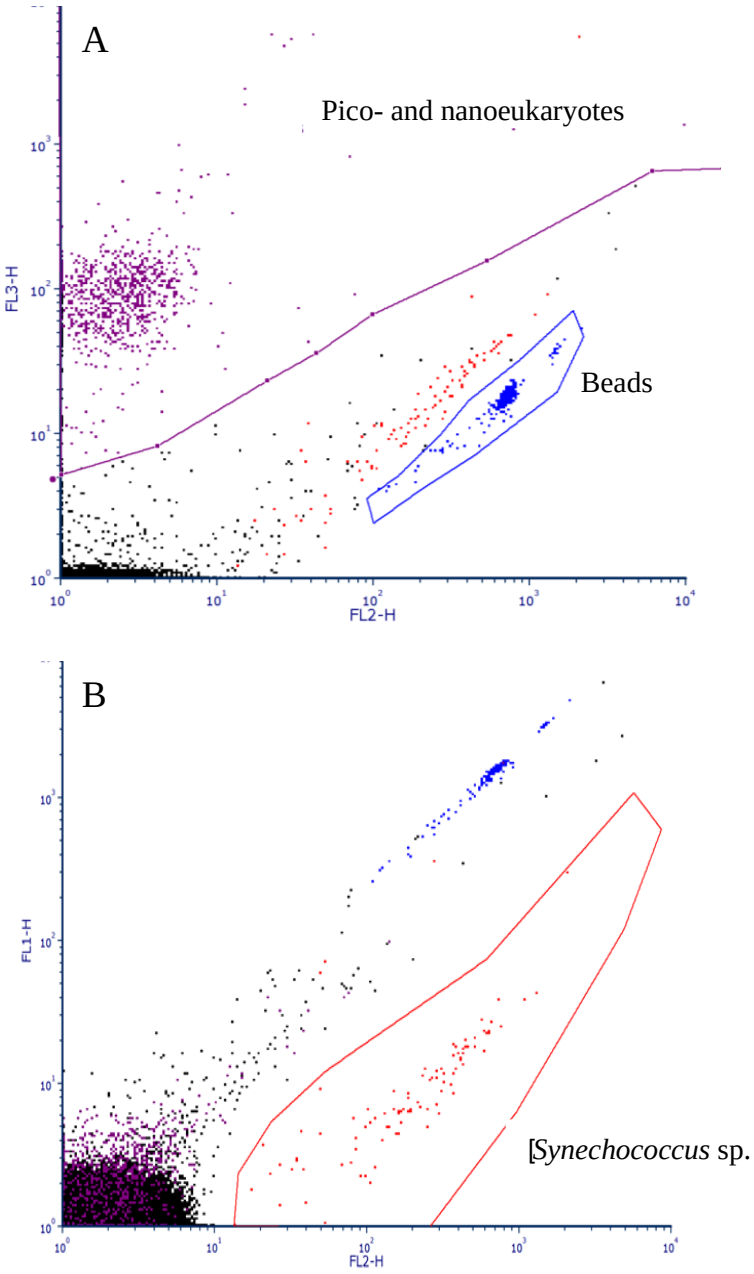

Figure S1. (A) Example pico- and nanoeukaryote and (B) *Synechococcus* sp. regions defined on FL2 v. FL3 and FL2 v. FL1 cytograms, respectively. Beads used to standardize fluorescence values and determine cell concentrations are shown in blue. Note debris in the bottom left corner of the plots, extending from bottom-left to top-right.

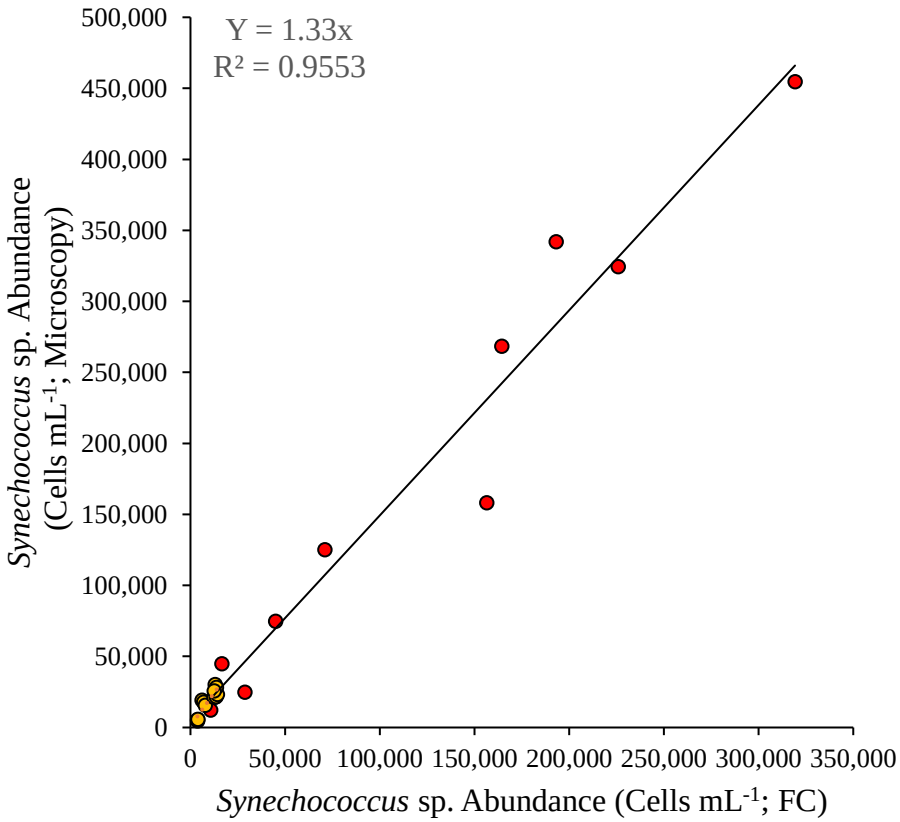

Figure S2. Correction of *Synechococcus* sp. abundances measured on LTER transects. LTER samples are shown in red, while iron addition samples are shown in orange. Linear regression of *Synechococcus* sp. abundances derived from flow cytometry and microscopy indicates that flow cytometry underestimated abundance. The regression slope was used to correct *Synechococcus* sp. abundances for LTER (shown here) and flow cytometry estimates (not shown).

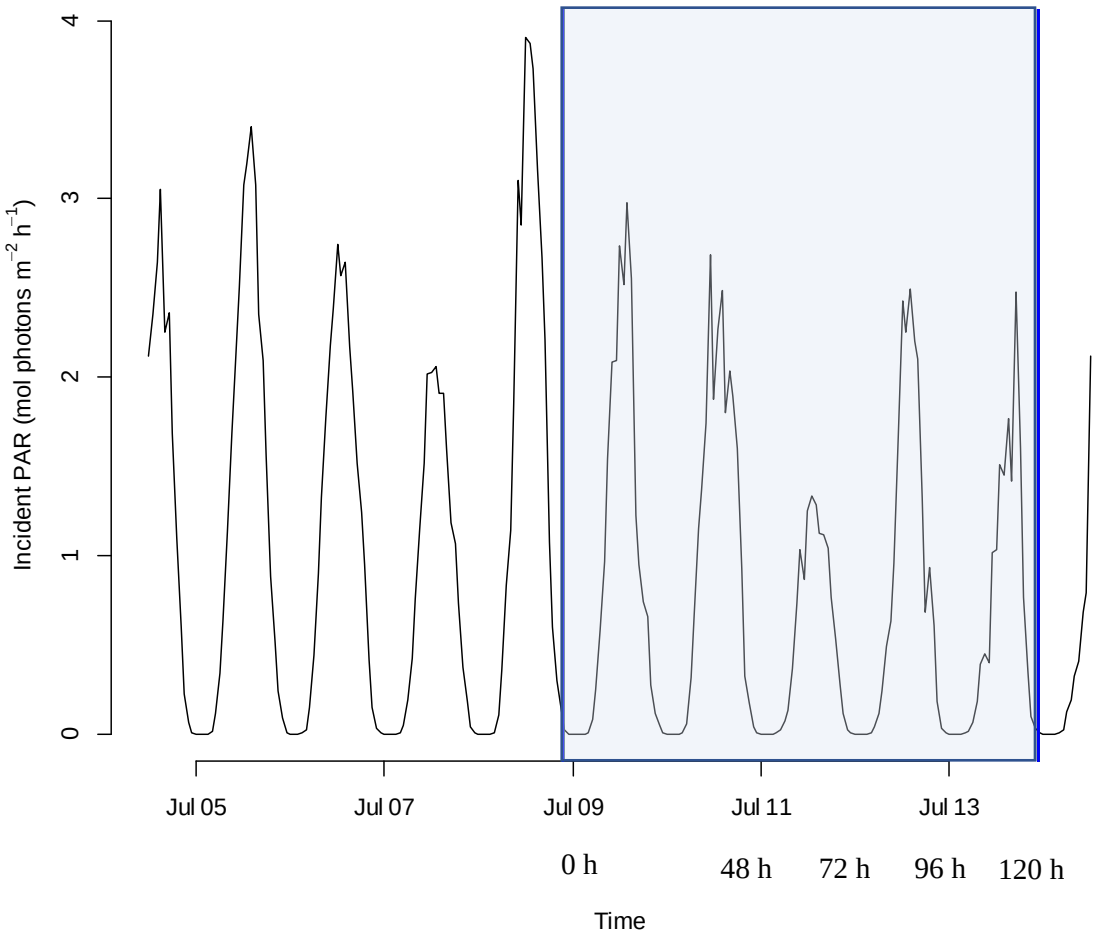

Figure S3. Incident PAR (µmol photons m^{-2} h^{-1}) before and during the iron addition experiment. The shaded box highlights PAR during the 5 d incubation.